Mathematical Problems in Engineering

Artificial Intelligence-Based Mathematical Modeling in Engineering: Recent Advances and Applications

Lead Guest Editor: Peiying Zhang
Guest Editors: Muhammad Zakarya and Haotong Cao

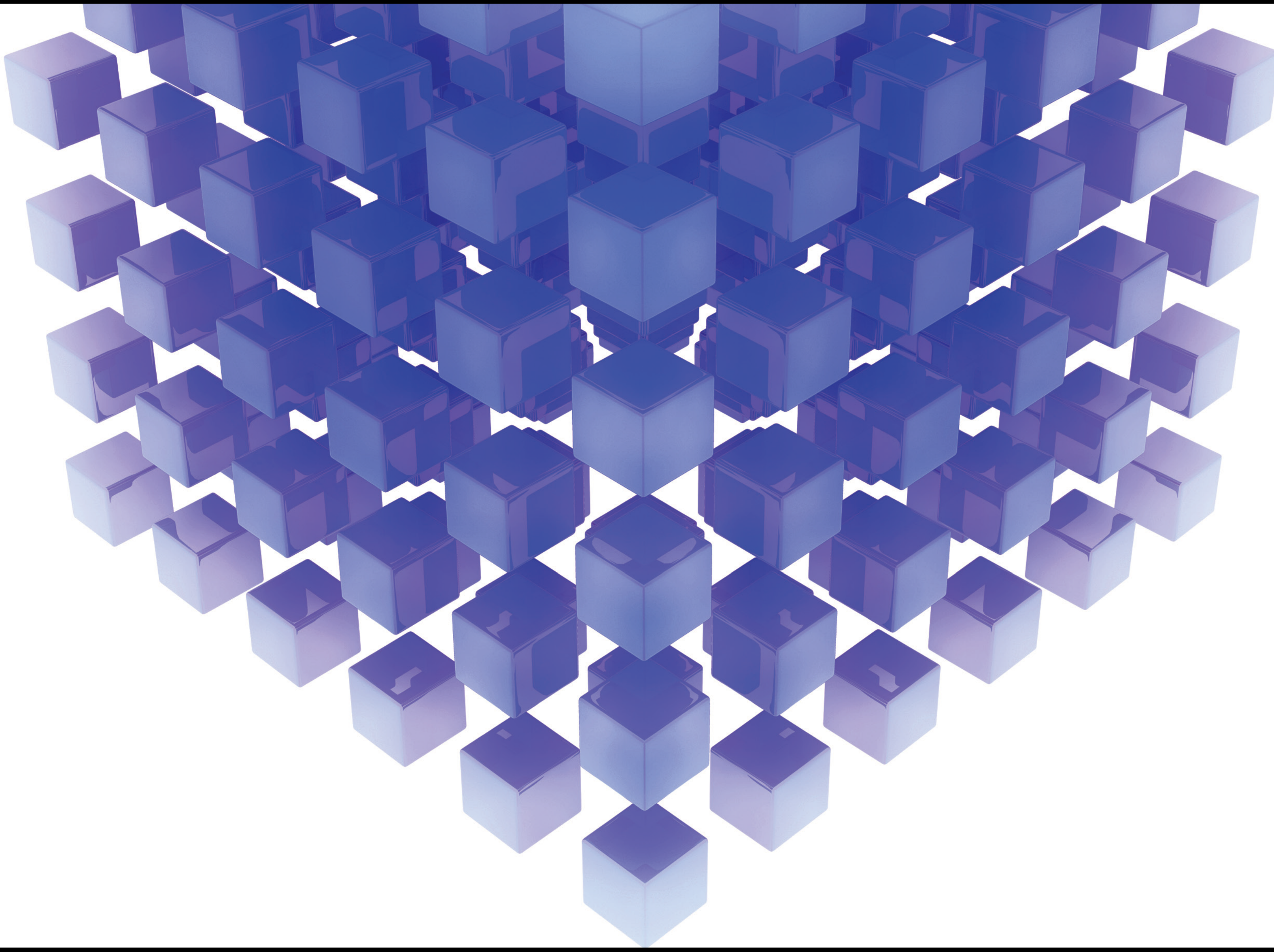

Artificial Intelligence-Based Mathematical Modeling in Engineering: Recent Advances and Applications

Mathematical Problems in Engineering

Artificial Intelligence-Based Mathematical Modeling in Engineering: Recent Advances and Applications

Lead Guest Editor: Peiying Zhang
Guest Editors: Muhammad Zakarya and Haotong Cao

Paolo Boscariol, Italy
Daniela Boso, Italy
Guillermo Botella-Juan, Spain
Abdesselem Boulkroune, Algeria
Boulaïd Boulkroune, Belgium
Fabio Bovenga, Italy
Francesco Braghin, Italy
Ricardo Branco, Portugal
Julien Bruchon, France
Matteo Bruggi, Italy
Michele Brun, Italy
Maria Elena Bruni, Italy
Maria Angela Butturi, Italy
Bartłomiej Błachowski, Poland
Dhanamjayulu C, India
Raquel Caballero-Águila, Spain
Filippo Cacace, Italy
Salvatore Caddemi, Italy
Zuowei Cai, China
Roberto Caldelli, Italy
Francesco Cannizzaro, Italy
Maosen Cao, China
Ana Carpio, Spain
Rodrigo Carvajal, Chile
Caterina Casavola, Italy
Sara Casciati, Italy
Federica Caselli, Italy
Carmen Castillo, Spain
Inmaculada T. Castro, Spain
Miguel Castro, Portugal
Giuseppe Catalanotti, United Kingdom
Alberto Cavallo, Italy
Gabriele Cazzulani, Italy
Fatih Vehbi Celebi, Turkey
Miguel Cerrolaza, Venezuela
Gregory Chagnon, France
Ching-Ter Chang, Taiwan
Kuei-Lun Chang, Taiwan
Qing Chang, USA
Xiaoheng Chang, China
Prasenjit Chatterjee, Lithuania
Kacem Chehdi, France
Peter N. Cheimets, USA
Chih-Chiang Chen, Taiwan
He Chen, China
Kebing Chen, China
Mengxin Chen, China
Shyi-Ming Chen, Taiwan
Xizhong Chen, Ireland
Xue-Bo Chen, China
Zhiwen Chen, China
Qiang Cheng, USA
Zeyang Cheng, China
Luca Chiapponi, Italy
Francisco Chicano, Spain
Tirivanhu Chinyoka, South Africa
Adrian Chmielewski, Poland
Seongim Choi, USA
Gautam Choubey, India
Hung-Yuan Chung, Taiwan
Yusheng Ci, China
Simone Cinquemani, Italy
Roberto G. Citarella, Italy
Joaquim Ciurana, Spain
John D. Clayton, USA
Piero Colajanni, Italy
Giuseppina Colicchio, Italy
Vassilios Constantoudis, Greece
Enrico Conte, Italy
Alessandro Contento, USA
Mario Cools, Belgium
Gino Cortellessa, Italy
Carlo Cosentino, Italy
Paolo Crippa, Italy
Erik Cuevas, Mexico
Guozeng Cui, China
Mehmet Cunkas, Turkey
Giuseppe D'Aniello, Italy
Peter Dabnichki, Australia
Weizhong Dai, USA
Zhifeng Dai, China
Purushothaman Damodaran, USA
Sergey Dashkovskiy, Germany
Adiel T. De Almeida-Filho, Brazil
Fabio De Angelis, Italy
Samuele De Bartolo, Italy
Stefano De Miranda, Italy
Filippo De Monte, Italy

José António Fonseca De Oliveira Correia, Portugal
Jose Renato De Sousa, Brazil
Michael Defoort, France
Alessandro Della Corte, Italy
Laurent Dewasme, Belgium
Sanku Dey, India
Gianpaolo Di Bona, Italy
Roberta Di Pace, Italy
Francesca Di Puccio, Italy
Ramón I. Diego, Spain
Yannis Dimakopoulos, Greece
Hasan Dinçer, Turkey
José M. Domínguez, Spain
Georgios Dounias, Greece
Bo Du, China
Emil Dumic, Croatia
Madalina Dumitriu, United Kingdom
Premraj Durairaj, India
Saeed Eftekhar Azam, USA
Said El Kafhali, Morocco
Antonio Elipe, Spain
R. Emre Erkmen, Canada
John Escobar, Colombia
Leandro F. F. Miguel, Brazil
FRANCESCO FOTI, Italy
Andrea L. Facci, Italy
Shahla Faisal, Pakistan
Giovanni Falsone, Italy
Hua Fan, China
Jianguang Fang, Australia
Nicholas Fantuzzi, Italy
Muhammad Shahid Farid, Pakistan
Hamed Faroqi, Iran
Yann Favennec, France
Fiorenzo A. Fazzolari, United Kingdom
Giuseppe Fedele, Italy
Roberto Fedele, Italy
Baowei Feng, China
Mohammad Ferdows, Bangladesh
Arturo J. Fernández, Spain
Jesus M. Fernandez Oro, Spain
Francesco Ferrise, Italy
Eric Feulvarch, France
Thierry Floquet, France
Eric Florentin, France
Gerardo Flores, Mexico
Antonio Forcina, Italy
Alessandro Formisano, Italy
Francesco Franco, Italy
Elisa Francomano, Italy
Juan Frausto-Solis, Mexico
Shujun Fu, China
Juan C. G. Prada, Spain
HECTOR GOMEZ, Chile
Matteo Gaeta, Italy
Mauro Gaggero, Italy
Zoran Gajic, USA
Jaime Gallardo-Alvarado, Mexico
Mosè Gallo, Italy
Akemi Gálvez, Spain
Maria L. Gandarias, Spain
Hao Gao, Hong Kong
Xingbao Gao, China
Yan Gao, China
Zhiwei Gao, United Kingdom
Giovanni Garcea, Italy
José García, Chile
Harish Garg, India
Alessandro Gasparetto, Italy
Stylianos Georgantzinos, Greece
Fotios Georgiades, India
Parviz Ghadimi, Iran
Ștefan Cristian Gherghina, Romania
Georgios I. Giannopoulos, Greece
Agathoklis Giaralis, United Kingdom
Anna M. Gil-Lafuente, Spain
Ivan Giorgio, Italy
Gaetano Giunta, Luxembourg
Jefferson L.M.A. Gomes, United Kingdom
Emilio Gómez-Déniz, Spain
Antonio M. Gonçalves de Lima, Brazil
Qunxi Gong, China
Chris Goodrich, USA
Rama S. R. Gorla, USA
Veena Goswami, India
Xunjie Gou, Spain
Jakub Grabski, Poland

Antoine Grall, France
George A. Gravvanis, Greece
Fabrizio Greco, Italy
David Greiner, Spain
Jason Gu, Canada
Federico Guarracino, Italy
Michele Guida, Italy
Muhammet Gul, Turkey
Dong-Sheng Guo, China
Hu Guo, China
Zhaoxia Guo, China
Yusuf Gurefe, Turkey
Salim HEDDAM, Algeria
ABID HUSSANAN, China
Quang Phuc Ha, Australia
Li Haitao, China
Petr Hájek, Czech Republic
Mohamed Hamdy, Egypt
Muhammad Hamid, United Kingdom
Renke Han, United Kingdom
Weimin Han, USA
Xingsi Han, China
Zhen-Lai Han, China
Thomas Hanne, Switzerland
Xinan Hao, China
Mohammad A. Hariri-Ardebili, USA
Khalid Hattaf, Morocco
Defeng He, China
Xiao-Qiao He, China
Yanchao He, China
Yu-Ling He, China
Ramdane Hedjar, Saudi Arabia
Jude Hemanth, India
Reza Hemmati, Iran
Nicolae Herisanu, Romania
Alfredo G. Hernández-Diaz, Spain
M.I. Herreros, Spain
Eckhard Hitzer, Japan
Paul Honeine, France
Jaromir Horacek, Czech Republic
Lei Hou, China
Yingkun Hou, China
Yu-Chen Hu, Taiwan
Yunfeng Hu, China
Can Huang, China
Gordon Huang, Canada
Linsheng Huo, China
Sajid Hussain, Canada
Asier Ibeas, Spain
Orest V. Iftime, The Netherlands
Przemyslaw Ignaciuk, Poland
Giacomo Innocenti, Italy
Emilio Insfran Pelozo, Spain
Azeem Irshad, Pakistan
Alessio Ishizaka, France
Benjamin Ivorra, Spain
Breno Jacob, Brazil
Reema Jain, India
Tushar Jain, India
Amin Jajarmi, Iran
Chiranjibe Jana, India
Łukasz Jankowski, Poland
Samuel N. Jator, USA
Juan Carlos Jáuregui-Correa, Mexico
Kandasamy Jayakrishna, India
Reza Jazar, Australia
Khalide Jbilou, France
Isabel S. Jesus, Portugal
Chao Ji, China
Qing-Chao Jiang, China
Peng-fei Jiao, China
Ricardo Fabricio Escobar Jiménez, Mexico
Emilio Jiménez Macías, Spain
Maolin Jin, Republic of Korea
Zhuo Jin, Australia
Ramash Kumar K, India
BHABEN KALITA, USA
MOHAMMAD REZA KHEDMATI, Iran
Viacheslav Kalashnikov, Mexico
Mathiyalagan Kalidass, India
Tamas Kalmar-Nagy, Hungary
Rajesh Kaluri, India
Jyotheeswara Reddy Kalvakurthi, India
Zhao Kang, China
Ramani Kannan, Malaysia
Tomasz Kapitaniak, Poland
Julius Kaplunov, United Kingdom
Konstantinos Karamanos, Belgium
Michal Kawulok, Poland

Francisco J. Martos, Spain
Elio Masciari, Italy
Paolo Massioni, France
Alessandro Mauro, Italy
Jonathan Mayo-Maldonado, Mexico
Pier Luigi Mazzeo, Italy
Laura Mazzola, Italy
Driss Mehdi, France
Zahid Mehmood, Pakistan
Roderick Melnik, Canada
Xiangyu Meng, USA
Jose Merodio, Spain
Alessio Merola, Italy
Mahmoud Mesbah, Iran
Luciano Mescia, Italy
Laurent Mevel, France
Constantine Michailides, Cyprus
Mariusz Michta, Poland
Prankul Middha, Norway
Aki Mikkola, Finland
Giovanni Minafò, Italy
Edmondo Minisci, United Kingdom
Hiroyuki Mino, Japan
Dimitrios Mitsotakis, New Zealand
Ardashir Mohammadzadeh, Iran
Francisco J. Montáns, Spain
Francesco Montefusco, Italy
Gisele Mophou, France
Rafael Morales, Spain
Marco Morandini, Italy
Javier Moreno-Valenzuela, Mexico
Simone Morganti, Italy
Caroline Mota, Brazil
Aziz Moukrim, France
Shen Mouquan, China
Dimitris Mourtzis, Greece
Emiliano Mucchi, Italy
Taseer Muhammad, Saudi Arabia
Ghulam Muhiuddin, Saudi Arabia
Amitava Mukherjee, India
Josefa Mula, Spain
Jose J. Muñoz, Spain
Giuseppe Muscolino, Italy
Marco Mussetta, Italy
Hariharan Muthusamy, India
Alessandro Naddeo, Italy
Raj Nandkeolyar, India
Keivan Navaie, United Kingdom
Soumya Nayak, India
Adrian Neagu, USA
Erivelton Geraldo Nepomuceno, Brazil
AMA Neves, Portugal
Ha Quang Thinh Ngo, Vietnam
Nhon Nguyen-Thanh, Singapore
Papakostas Nikolaos, Ireland
Jelena Nikolic, Serbia
Tatsushi Nishi, Japan
Shanzhou Niu, China
Ben T. Nohara, Japan
Mohammed Nouari, France
Mustapha Nourelfath, Canada
Kazem Nouri, Iran
Ciro Núñez-Gutiérrez, Mexico
Wlodzimierz Ogryczak, Poland
Roger Ohayon, France
Krzysztof Okarma, Poland
Mitsuhiro Okayasu, Japan
Murat Olgun, Turkey
Diego Oliva, Mexico
Alberto Olivares, Spain
Enrique Onieva, Spain
Calogero Orlando, Italy
Susana Ortega-Cisneros, Mexico
Sergio Ortobelli, Italy
Naohisa Otsuka, Japan
Sid Ahmed Ould Ahmed Mahmoud, Saudi Arabia
Taoreed Owolabi, Nigeria
EUGENIA PETROPOULOU, Greece
Arturo Pagano, Italy
Madhumangal Pal, India
Pasquale Palumbo, Italy
Dragan Pamučar, Serbia
Weifeng Pan, China
Chandan Pandey, India
Rui Pang, United Kingdom
Jürgen Pannek, Germany
Elena Panteley, France
Achille Paolone, Italy

George A. Papakostas, Greece
Xosé M. Pardo, Spain
You-Jin Park, Taiwan
Manuel Pastor, Spain
Pubudu N. Pathirana, Australia
Surajit Kumar Paul, India
Luis Payá, Spain
Igor Pažanin, Croatia
Libor Pekař, Czech Republic
Francesco Pellicano, Italy
Marcello Pellicciari, Italy
Jian Peng, China
Mingshu Peng, China
Xiang Peng, China
Xindong Peng, China
Yuexing Peng, China
Marzio Pennisi, Italy
Maria Patrizia Pera, Italy
Matjaz Perc, Slovenia
A. M. Bastos Pereira, Portugal
Wesley Peres, Brazil
F. Javier Pérez-Pinal, Mexico
Michele Perrella, Italy
Francesco Pesavento, Italy
Francesco Petrini, Italy
Hoang Vu Phan, Republic of Korea
Lukasz Pieczonka, Poland
Dario Piga, Switzerland
Marco Pizzarelli, Italy
Javier Plaza, Spain
Goutam Pohit, India
Dragan Poljak, Croatia
Jorge Pomares, Spain
Hiram Ponce, Mexico
Sébastien Poncet, Canada
Volodymyr Ponomaryov, Mexico
Jean-Christophe Ponsart, France
Mauro Pontani, Italy
Sivakumar Poruran, India
Francesc Pozo, Spain
Aditya Rio Prabowo, Indonesia
Anchasa Pramuanjaroenkij, Thailand
Leonardo Primavera, Italy
B Rajanarayan Prusty, India
Krzysztof Puszynski, Poland
Chuan Qin, China
Dongdong Qin, China
Jianlong Qiu, China
Giuseppe Quaranta, Italy
DR. RITU RAJ, India
Vitomir Racic, Italy
Carlo Rainieri, Italy
Kumbakonam Ramamani Rajagopal, USA
Ali Ramazani, USA
Angel Manuel Ramos, Spain
Higinio Ramos, Spain
Muhammad Afzal Rana, Pakistan
Muhammad Rashid, Saudi Arabia
Manoj Rastogi, India
Alessandro Rasulo, Italy
S.S. Ravindran, USA
Abdolrahman Razani, Iran
Alessandro Reali, Italy
Jose A. Reinoso, Spain
Oscar Reinoso, Spain
Haijun Ren, China
Carlo Renno, Italy
Fabrizio Renno, Italy
Shahram Rezapour, Iran
Ricardo Riaza, Spain
Francesco Riganti-Fulginei, Italy
Gerasimos Rigatos, Greece
Francesco Ripamonti, Italy
Jorge Rivera, Mexico
Eugenio Roanes-Lozano, Spain
Ana Maria A. C. Rocha, Portugal
Luigi Rodino, Italy
Francisco Rodríguez, Spain
Rosana Rodríguez López, Spain
Francisco Rossomando, Argentina
Jose de Jesus Rubio, Mexico
Weiguo Rui, China
Rubén Ruiz, Spain
Ivan D. Rukhlenko, Australia
Dr. Eswaramoorthi S., India
Weichao SHI, United Kingdom
Chaman Lal Sabharwal, USA
Andrés Sáez, Spain

Bekir Sahin, Turkey
Laxminarayan Sahoo, India
John S. Sakellariou, Greece
Michael Sakellariou, Greece
Salvatore Salamone, USA
Jose Vicente Salcedo, Spain
Alejandro Salcido, Mexico
Alejandro Salcido, Mexico
Nunzio Salerno, Italy
Rohit Salgotra, India
Miguel A. Salido, Spain
Sinan Salih, Iraq
Alessandro Salvini, Italy
Abdus Samad, India
Sovan Samanta, India
Nikolaos Samaras, Greece
Ramon Sancibrian, Spain
Giuseppe Sanfilippo, Italy
Omar-Jacobo Santos, Mexico
J Santos-Reyes, Mexico
José A. Sanz-Herrera, Spain
Musavarah Sarwar, Pakistan
Shahzad Sarwar, Saudi Arabia
Marcelo A. Savi, Brazil
Andrey V. Savkin, Australia
Tadeusz Sawik, Poland
Roberta Sburlati, Italy
Gustavo Scaglia, Argentina
Thomas Schuster, Germany
Hamid M. Sedighi, Iran
Mijanur Rahaman Seikh, India
Tapan Senapati, China
Lotfi Senhadji, France
Junwon Seo, USA
Michele Serpilli, Italy
Silvestar Šesnić, Croatia
Gerardo Severino, Italy
Ruben Sevilla, United Kingdom
Stefano Sfarra, Italy
Dr. Ismail Shah, Pakistan
Leonid Shaikhet, Israel
Vimal Shanmuganathan, India
Prayas Sharma, India
Bo Shen, Germany
Hang Shen, China
Xin Pu Shen, China
Dimitri O. Shepelsky, Ukraine
Jian Shi, China
Amin Shokrollahi, Australia
Suzanne M. Shontz, USA
Babak Shotorban, USA
Zhan Shu, Canada
Angelo Sifaleras, Greece
Nuno Simões, Portugal
Mehakpreet Singh, Ireland
Piyush Pratap Singh, India
Rajiv Singh, India
Seralathan Sivamani, India
S. Sivasankaran, Malaysia
Christos H. Skiadas, Greece
Konstantina Skouri, Greece
Neale R. Smith, Mexico
Bogdan Smolka, Poland
Delfim Soares Jr., Brazil
Alba Sofi, Italy
Francesco Soldovieri, Italy
Raffaele Solimene, Italy
Yang Song, Norway
Jussi Sopanen, Finland
Marco Spadini, Italy
Paolo Spagnolo, Italy
Ruben Specogna, Italy
Vasilios Spitas, Greece
Ivanka Stamova, USA
Rafał Stanisławski, Poland
Miladin Stefanović, Serbia
Salvatore Strano, Italy
Yakov Strelniker, Israel
Kangkang Sun, China
Qiuqin Sun, China
Shuaishuai Sun, Australia
Yanchao Sun, China
Zong-Yao Sun, China
Kumarasamy Suresh, India
Sergey A. Suslov, Australia
D.L. Suthar, Ethiopia
D.L. Suthar, Ethiopia
Andrzej Swierniak, Poland
Andras Szekrenyes, Hungary
Kumar K. Tamma, USA

Yong (Aaron) Tan, United Kingdom
Marco Antonio Taneco-Hernández, Mexico
Lu Tang, China
Tianyou Tao, China
Hafez Tari, USA
Alessandro Tasora, Italy
Sergio Teggi, Italy
Adriana del Carmen Téllez-Anguiano, Mexico
Ana C. Teodoro, Portugal
Efstathios E. Theotokoglou, Greece
Jing-Feng Tian, China
Alexander Timokha, Norway
Stefania Tomasiello, Italy
Gisella Tomasini, Italy
Isabella Torcicollo, Italy
Francesco Tornabene, Italy
Mariano Torrisi, Italy
Thang nguyen Trung, Vietnam
George Tsiatas, Greece
Le Anh Tuan, Vietnam
Nerio Tullini, Italy
Emilio Turco, Italy
Ilhan Tuzcu, USA
Efstratios Tzirtzilakis, Greece
FRANCISCO UREÑA, Spain
Filippo Ubertini, Italy
Mohammad Uddin, Australia
Mohammad Safi Ullah, Bangladesh
Serdar Ulubeyli, Turkey
Mati Ur Rahman, Pakistan
Panayiotis Vafeas, Greece
Giuseppe Vairo, Italy
Jesus Valdez-Resendiz, Mexico
Eusebio Valero, Spain
Stefano Valvano, Italy
Carlos-Renato Vázquez, Mexico
Martin Velasco Villa, Mexico
Franck J. Vernerey, USA
Georgios Veronis, USA
Vincenzo Vespri, Italy
Renato Vidoni, Italy
Venkatesh Vijayaraghavan, Australia
Anna Vila, Spain
Francisco R. Villatoro, Spain
Francesca Vipiana, Italy
Stanislav Vítek, Czech Republic
Jan Vorel, Czech Republic
Michael Vynnycky, Sweden
Mohammad W. Alomari, Jordan
Roman Wan-Wendner, Austria
Bingchang Wang, China
C. H. Wang, Taiwan
Dagang Wang, China
Guoqiang Wang, China
Huaiyu Wang, China
Hui Wang, China
J.G. Wang, China
Ji Wang, China
Kang-Jia Wang, China
Lei Wang, China
Qiang Wang, China
Qingling Wang, China
Weiwei Wang, China
Xinyu Wang, China
Yong Wang, China
Yung-Chung Wang, Taiwan
Zhenbo Wang, USA
Zhibo Wang, China
Waldemar T. Wójcik, Poland
Chi Wu, Australia
Qiuhong Wu, China
Yuqiang Wu, China
Zhibin Wu, China
Zhizheng Wu, China
Michalis Xenos, Greece
Hao Xiao, China
Xiao Ping Xie, China
Qingzheng Xu, China
Binghan Xue, China
Yi Xue, China
Joseph J. Yame, France
Chuanliang Yan, China
Xinggang Yan, United Kingdom
Hongtai Yang, China
Jixiang Yang, China
Mijia Yang, USA
Ray-Yeng Yang, Taiwan

Contents

Hindawi
Mathematical Problems in Engineering
Volume 2023, Article ID 4176997, 12 pages
https://doi.org/10.1155/2023/4176997

Research Article

An Experimental Testing of Optimized Fuzzy Logic-Based MPPT for a Standalone PV System Using Genetic Algorithms

Fatah Yahiaoui,[1] Ferhat Chabour,[2] Ouahib Guenounou,[1] Mohit Bajaj,[3,4,5] Syed Sabir Hussain Bukhari,[6] Muhammad Shahzad Nazir ,[7] Mukesh Pushkarna,[8] and Daniel Eutyche Mbadjoun Wapet [9]

[1]*Laboratoire de Technologie Industrielle et de l'Information (LTII), Faculté de Technologie, Université de Béjaïa, Béjaïa 06000, Algeria*
[2]*GREAH Laboratory, University of Le Havre, 25 Rue Philippe Lebon, Le Havre 76600, France*
[3]*Department of Electrical Engineering, Graphic Era (Deemed to be University), Dehradun 248002, India*
[4]*Graphic Era Hill University, Dehradun 248002, India*
[5]*Applied Science Research Center, Applied Science Private University, Amman 11931, Jordan*
[6]*School of Electrical and Electronics Engineering, Chung-Ang University, Dongjak-gu, Seoul 06974, Republic of Korea*
[7]*Faculty of Automation, Huaiyin Institute of Technology, Huai'an 223003, China*
[8]*Department of Electrical Engineering, GLA University, Mathura 281406, India*
[9]*National Advanced School of Engineering, Université de Yaoundé I, Yaoundé, Cameroon*

Correspondence should be addressed to Daniel Eutyche Mbadjoun Wapet; eutychedan@gmail.com

Received 7 October 2022; Revised 28 December 2022; Accepted 9 April 2023; Published 27 April 2023

Academic Editor: Ardashir Mohammadzadeh

The choice and the dimensioning of the controller for the maximum power point tracking (MPPT) are determined for the ideal energy efficiency of the photovoltaic (PV) systems. Many works have been developed in the field of MPPT methods, especially fuzzy logic controllers. However, these are robust if the parameters of the membership functions have been well designed. In this paper, the performances of an intelligent fuzzy logic controller (FLC)-based MPPT method have been optimized by an evolutionary genetic algorithm (GA). The works presented in the literature have shown the efficiency of the proposed method compared to classical methods. In our paper, the validation of the experimental results obtained is given with respect to a reference signal. The control of the simulated PV source and the proposed method are built using the Simulink/Matlab environment and implemented on the dSPACE DS1104 controller to validate the practical execution of the suggested method. The standalone PV system has been tested in an emulated test bench experimentation. Experimental results confirm the efficiency of the proposed method and its high accuracy in handling fast varying load conditions.

1. Introduction

Renewable energy is critical to sustainable development around the globe. Photovoltaic (PV) energy is one of the most abundantly available and cost-effective renewable energy sources. PV power is utilized in grid-integrated, standalone, and hybrid energy systems [1]. Standalone PV systems are utilized in distant locations where power from the main AC grids is not available. PV systems that include an energy storage system. PV power is also integrated into a grid using power converters, and in order to meet the standards of grid codes, the integration of such power source needs sophisticated control techniques. Hybrid power systems can be produced by combining solar photovoltaic systems with wind, tidal, and thermal energy [2]. However, due to the stochastic nature of solar/PV energy, the output power produced by PV systems is also fluctuating.

The solar panel can give the maximum amount of power to the load at its ideal operating point. Maximum power point (MPP) is the common name for the specific operating point. Because solar irradiation and cell temperature have a significant impact on the current-voltage characteristic of PV modules, the locus of MPP exhibits nonlinear change. The MPPT is to be created for the PV system due to the nonlinearity of PV modules. At any solar irradiation and temperature, MPPT is able to determine the PV panel MPP operating voltage. The PV system controls the PV module's voltage to the MPP operating voltage. It is possible to draw as much power as you can. As a result, the PV system's effectiveness can be increased [2, 3].

Several research algorithms have been reported to extract the maximum power from solar panels under stochastic environmental conditions. A number of techniques have been presented in recent years as examples, including perturb and observe (P&O) [4], incremental conductance (INC) [5], and fuzzy logic controller (FLC) [6].

The simplest algorithms are P&O and INC. However, due to the fact that the disturbance continues even when the system is functioning at the MPP, these techniques lead to power oscillations around the MPP. The duty cycle step might be decreased to address this problem. However, in this scenario, as atmospheric circumstances change, the system will track the MPP slowly. The PV system's total efficiency is decreased as a result of the power losses. A slight change in the step size in the P&O algorithm disrupts algorithm control. The measurement of PV system output power causes a slight modification to the direction of the step size specified by the P&O technique. Common problems could occur if a PV panel's output power is increased or decreased abruptly [7].

Alternatively, the FLC is used to track an MPP with more accuracy due to its inherent advantages in handling nonlinearity and the lack of a mathematical model, but this algorithm is greatly related to user experience with the PV panel characteristics. As reported in [8], an MPPT algorithm based on the FLC has been applied successfully for a photovoltaic generator system with a variable resistive. From the presented results, the FLC-based MPPT algorithm ensured enhanced performance as compared to the P&O technique. Similarly, in [9], an FLC-based MPPT controller is tested under variable atmospheric conditions. The FLC MPPT controller proposed in [9] guaranteed the optimal operation and performance of the autonomous PV system. In [10, 11], authors reported fuzzy controllers to regulate the power generated in a hybrid system containing PV and wind turbine systems. The study of interval type-3 fuzzy logic controllers (IT3 FLCs) has gotten a lot of attention recently. Numerous studies have demonstrated that IT3 FLCs can manage uncertainties better than their type-1 (T1) and type-2 (T2) counterparts [12].

Even though FLC controllers have many advantages, building them is still challenging since there is no standardized method for locating fuzzy control rules and fine-tuning the membership function parameters of the controllers. To get the better of this limitation, the design procedures are formulated as optimization problems that are typically solved using evolutionary algorithms [13–15], such as genetic algorithms (GAs). GAs are widely regarded as one of the most effective optimization techniques. The GA is capable of solving a wide range of complex optimization problems, including those with nonderivable cost functions [16]. Genetic algorithms attempt to simulate the evolutionary process of species in their natural environment: an artificial transposition of basic concepts of genetics and the laws of survival stated by Darwin.

A GA is constructed in quite analogous way. In the solution set of an optimization problem, a population of size N consists of N solutions (the individuals in the population) suitably marked by coding that identifies them completely. An evaluation procedure is necessary to determine the strength of each individual in the population. Then, there is a selection phase (in which individuals are chosen in proportion to their strength) and a recombination phase (in which artificial operators of crossing and mutation are used to generate a new population of individuals with a good chance of being stronger than those in the previous generation). From generation to generation, the strength of the individuals in the population increases, and after a certain number of iterations, the population is entirely composed of strong individuals, that is to say, of quasi-optimal solutions to the problem.

Theoretical work on the optimization problem of fuzzy controllers has been widely reported in the literature. A GA-based optimization problem is solved in [17] to find the optimal scaling parameters of a fuzzy logic-based MPPT controller that maximizes the efficiency of a PV pumping system. In [18], the algorithm GA is used to optimize the following two controllers: the fuzzy PI (proportional and integrator) and the P&O PI. The simulation results presented in this article have demonstrated that the fuzzy PI-GA is better than the P&O PI-GA in terms of response time. Similarly, in [19], theoretical simulations have been carried out. The authors have used a hierarchical genetic algorithm to design a fuzzy controller for the command of a photovoltaic conversion system.

The implementation aspect of optimized fuzzy controllers has been reported in [20–25]. An experimental study on the MPPT controller using the FPGA (field programmable gate array) has been presented in [21]. Based on the obtained results, the authors concluded that the optimized FLC outperforms the conventional P&O method in terms of response time and steady-state fluctuations. In [23], FPGA implementation of MPPT-based fuzzy logic is investigated for standalone PV conversion systems. In [24], FPGA implementation of a fuzzy controller is reported for a PV system. The authors in [25] discuss the MPPT technique based on GAs for a standalone PV conversion system. The results have been compared with the conventional techniques. The results have been validated experimentally using a dSPACE control board. Another two hardware implementations of fuzzy controllers for MPPT of PV systems have been described in recent works [26, 27]. The experimental results obtained have been compared to a conventional P&O method. The fuzzy controller design has been better than the P&O. However, it shows significant oscillations at the optimal point.

This paper discusses the hardware implementation of a fuzzy controller optimized by the GA algorithm for MPPT tracking using the dSPACE 1104 control board. The proposed MPPT method is tested for maximum harvesting power under real-time environmental conditions. The following is a summary of the primary differences between the current work and the related literature:

(i) The fuzzy controller is optimized to improve the convergence speed for maximum power harvesting of the PV system. The suggested technique can also track the global MPP (GMPP) efficiently, which is very beneficial in variable atmospheric conditions.

(ii) The proposed algorithm is tested for fast-changing solar irradiation and a variable resistance load.

(iii) In the cited literature [20–25], the design of a fuzzy MPPT controller using the GA optimization algorithm is accomplished for a learning profile of constant conditions ($T = 25°C$ and $S = 1000\,W/m^2$). However, atmospheric conditions are constantly changing. In this work, different variations of the irradiance ($600\,W/m^2$, $1000\,W/m^2$, and $800\,W/m^2$) are adopted to test the robustness of the optimized control utilized.

The paper's sections are structured as follows: Section 2 is a description of the system. Section 3 shows the design procedures of the fuzzy controller. Section 4 shows the proposed optimized control strategy. Section 5 presents the steps of the details of the experimental real-time platform. The result discussion is also presented in this section. Finally, Section 6 presents a general conclusion that will summarize the content of this work and put forward the results obtained.

2. Standalone PV System Description

Figure 1 shows a block diagram of a standalone PV system. The components of the system are the PV panel connected to a variable resistive load through a matching stage. The latter is composed of a boost converter. The switch of the converter is controlled by the signals generated by the proposed method.

2.1. PV Panel Model's Mathematical Equation. There are a few different sorts of models, such as single-diode and two-diode models [28, 29]. The two-diode model accounts for a second diode that is wired in parallel with the first diode in the circuit that functions as a single diode's equivalent. Compared to a two-diode model, the one-diode model has fewer parameters and is simpler to model. The electrical properties P (V) and I (V) of the solar panel as simulated and experimental data clearly demonstrate that the results are identical, according to the paper [29]. The one-diode model of the solar cell is used in this paper [29].

The PV panel model's mathematical equation is formulated according to the cell's number in series only, and the cell's number in parallel is equal to 1 according to our BP SX150S model in the following equation:

$$I_{pv} = I_{Ph} - I_s\left(\exp\left(\frac{V_{pv} + I_{pv}R_s}{N_s V_T}\right) - 1\right) - \left(\frac{V_{pv} + I_{pv}R_s}{R_{sh}}\right), \quad (1)$$

where V_T is equal to $(a.k.T/q)$.

The PV panel electrical parameters shown in equation (1) are reported in Table 1.

Table 2 lists the BP SX150S solar panel from BP solar, which is reported at the Standard Test Condition (STC, i.e., 25°C and $1000\,W/m^2$).

2.2. Boost Power Converter. The boost power converter is inserted between the PV panel and the load as an impedance-matching stage. The PV output voltage (V_{pv}) is regulated to keep it at the nominal voltage (V_{MPP}) by means of an MPPT controller. Voltage regulation is equivalent to controlling the opening and closing of the IGBT power switch through a pulse width modulation (PWM) technology. The IGBT switching frequency is 8 kHz.

To get the most power out of the PV panel that is now available, a new duty ratio D of the PWM signal must be generated in real-time. Table 3 lists the parameter values for the boost converter that was designed. The mathematical equation of the boost converter's output voltage and current has been given as follows [30]:

$$\begin{cases} V_o = \dfrac{1}{1-D} V_i, \\ I_o = (1-D) I_i, \end{cases} \quad (2)$$

where V_o and I_o are the output's voltages and currents of boost converters, respectively, and V_i and I_i are the input's voltages and currents of boost converters, respectively.

3. Fuzzy MPPT Controller

The fuzzy MPPT controller is an intelligent method of tracking a PV system's maximum power point. In lieu of a precise mathematical model, it uses the fuzzy set theory. The internal functioning of a fuzzy controller of the Mamdani type is based on the structure presented in Figure 2, which includes four blocks [31].

The fuzzification consists in calculating, for each real input value, the degrees of membership to the associated fuzzy sets predefined in the database of the fuzzy system. This block carries out the transformation of the real inputs into symbolic information that can be used by the inference mechanism.

The inference mechanism consists, on the one hand, in calculating the degree of truth of the different rules of the system and, on the other hand, in associating an output value to each of these rules. This output value depends on the conclusion part of the rules, which can take several forms. It can be a fuzzy proposition, and we will speak of a rule of type Mamdani "IF-THEN" in this case:

$$\text{IF } (\ldots) \text{ THEN } Y \textit{ is } X,\ X \text{ is set flou}. \quad (3)$$

The defuzzification consists in replacing the set of output values of the various rules resulting from the inference by a single real value representative of this set.

The inputs and outputs of the FLC controller are represented by the triangular and trapezoidal MFs. In Table 4, the letters P and N stand for positive and negative linguistic

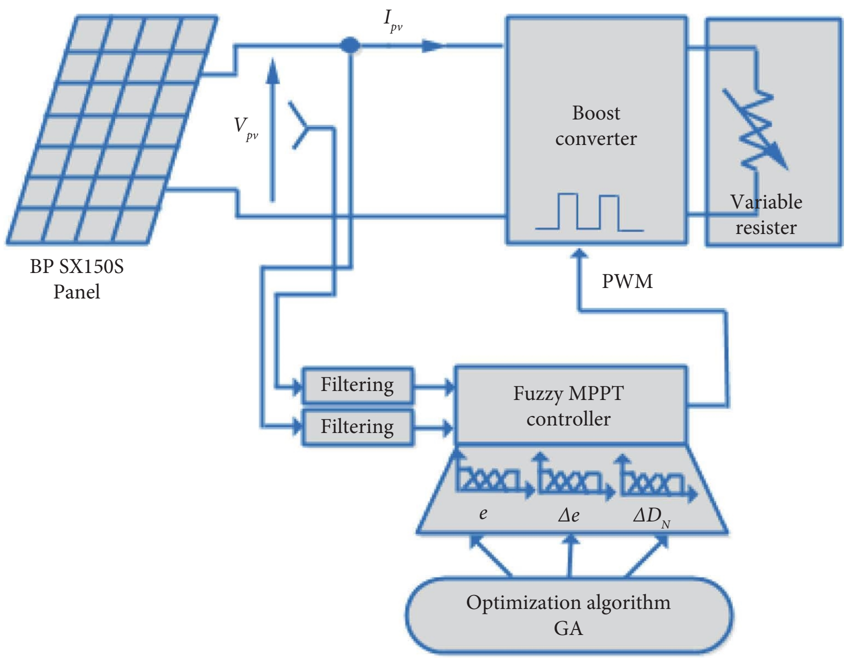

Figure 1: The illustrative diagram of the implemented PV system.

Table 1: PV panel electrical parameters.

Parameters	Designations
V_T	Diode thermal voltage
a	Diode ideality factor
K	Boltzmann constant
T	Cell's temperature
Q	Electron charge
I_{Ph}	Light generated current
I_s	Diode saturation current
R_s	Series equivalent resistances
R_{sh}	Parallel equivalent resistances

variables, respectively. The letters B, S, and ZE additionally stand for Big, Small, and Zero. Five separate linguistic variables are allocated to each input variable, $e(k)$ and $e(k)$. As a result, there are 25 different fuzzy rules in the suggested set of fuzzy rules. The entire set of fuzzy rules is presented in Table 4 [31].

The two input variables that are characterized by the following expressions at a sampling instant k are the error equation (4) and error variation equation (5):

$$e(k) = \frac{P_{\mathrm{pv}}(k) - P_{\mathrm{pv}}(k-1)}{V_{\mathrm{pv}}(k) - V_{\mathrm{pv}}(k-1)}, \tag{4}$$

$$\Delta e(k) = e(k) - e(k-1). \tag{5}$$

Based on these two inputs, the FLC calculates the subsequent operating point using MFs and a rule table. The operating point will be on the right or left side of the MPP, depending on whether E is positive or negative. When E equals zero, the MPP is reached. The operational point moves in the MPP direction according to the e-input.

The duty ratio D is computed as follows:

Table 2: The BP SX150S solar panel.

Parameters	
Nominal power (P_{MPP})	150 W
Output power tolerance	± 5%
Nominal current (I_{MPP})	4.35 A
Nominal voltage (V_{MPP})	34.5 V
Open circuit voltage (V_{oc})	43.5 V
Short circuit current (I_{sc})	4.75 A
Cells number in series (N_s)	72

Table 3: DC-DC boost converter specifications.

Electrical specifications	
Inductor (L)	0.6 mH
Input capacitor (C_i)	500 μF
Output capacitor (C_o)	2200 μF
Switching frequency (f_s)	8 kHz
IGBT	SKM50GB12T4

$$D(k) = G_D \times \Delta D_N(k) + D(k-1), \tag{6}$$

where ΔD_N is the duty ratio at the controller output and G_D represents the factor's scaling output.

4. Proposed Optimized Fuzzy-Based MPPT

Generally speaking, the following steps can be used to define the genetic algorithm.

4.1. Procedure Genetic Algorithm

Step 1 (initialization). Generate an initial population Pop (t) of size N of chromosomes in a random manner.

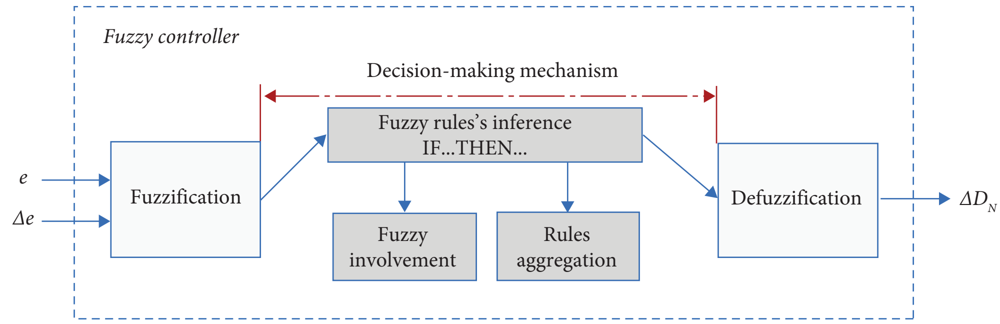

Figure 2: The synoptic diagram of a fuzzy controller.

Table 4: The rule base table for the fuzzy MPPT controller.

e	Δe NB	NS	ZE	PS	PB
NB	ZE	ZE	PB	PB	PB
NS	ZE	ZE	PS	PS	PS
ZE	PS	ZE	ZE	ZE	NS
PS	NS	NS	NS	ZE	ZE
PB	NB	NB	NB	ZE	ZE

Step 2 (evaluation). Each chromosome is decoded and evaluated Pop (t).

Step 3 (Selection). Production of a new population of N chromosomes with the use of a suitable selection technique, select Pop (t) from Pop (t-1).

Step 4 (recombination). According to their probability, crossover, and mutation of some chromosomes within the new population.

Step 5 (termination). To phase 2, as long as the problem stop condition is not satisfied.

4.2. Structure of Chromosomes. In this paper, the membership functions of the fuzzy MPPT controller are optimized. The inputs and output membership functions are each defined by five parameters. For a fuzzy controller with two input variables and one output variable, the membership function numbers are in order 3×5. Therefore, the GA chromosome's structure is given as a vector of fifteen parameter values, as shown in Figure 3.

4.3. Initial Population. The chromosomes of the original population are set to random variables. A sequence of random numbers $r_{i,j}$ between 0 and 1 is created for each element $X_{i,j}$ of particle i. Then, by projecting [0, 1] into $[X_j^L, X_j^U]$, $X_{i,j}$ is determined as follows:

$$X_{i,j} = X_j^L + r_{i,j} \times \left(X_j^U - X_j^L\right), \tag{7}$$

where X_j^L represents the inferior limit of $X_{i,j}$ and X_j^U represents the upper limit of $X_{i,j}$.

4.4. Optimization Criterion. The goal of designing a fuzzy MPPT controller is to discover the optimal settings that minimize energy loss in the PV system, which is mostly caused by meteorological conditions. The optimization criterion's objective function given in equation (8) describes an integral squared error (ISE) function. At each learning step, an ISE value is calculated, and at the end, the best value is returned.

$$ISE = \int_0^{t_f} (e(t))^2 \mathrm{d}t, \tag{8}$$

where $e(t) = P_{\max}(t) - P_{\mathrm{pv}}(t)$, $P_{\max}$ is the PV panel's rated power, P_{pv} is the PV panel's instant power, and t_f is the simulation time.

4.5. Selection Process. The selection process is applied to the chromosomes of the algorithm. This process is the first step in the selection of the best chromosomes suitable for replication. The tournament selection is used in this work. This selection technique uses proportional selection on chromosome's pairs and then chooses from these pairs the chromosome with the best adaptation (fitness) score.

4.6. Crossover and Mutation Operators. In this study, for a real-coded genetic algorithm, the Laplace crossover operator is suggested [32, 33]. For the real string, a real value mutation has been created. Each parameter $X_{i,j}$ receives an addition of a random with the probability rate pm. The direct application of this mutation can create new parameters outside the interval $[X_j^L, X_j^U]$. Therefore, we propose the following mutation equation (9) for keeping parameters in their range of variation:

$$X_{i,j} = \begin{cases} X_{i,j} + \mathrm{rand}_1 \times \left(X_j^U - X_{i,j}\right) \text{ if } \mathrm{rand}_3 < 0.5, \\ X_{i,j} + \mathrm{rand}_2 \times \left(X_j^L - X_{i,j}\right) \text{ if } \mathrm{rand}_3 \geq 0.5, \end{cases} \tag{9}$$

where rand_1, rand_2, and rand_3 are random numbers between [0, 1].

5. Experimental Results and Discussion

The experimental test bench for the simulated PV system is depicted in Figure 4. The GREAH laboratory in France is where the hardware implementation was developed. The implementation in real time of the proposed MPPT

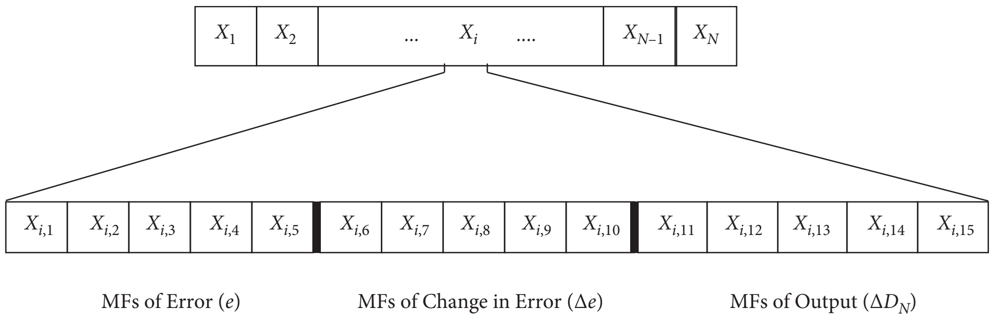

Figure 3: The N chromosome's real coding structure.

controller has been given by a dSPACE DS1104 board. The Simulink model of the PV panel as well as the solar radiation and temperature profiles were implemented on a Dspace 1104 board. The reference current and voltage signals computed by the panel control an adjustable DC power supply. Figure 5(a) shows the acquisition chain of the PV source emulator (EPVS). The emulated system involves the use of a boost converter to connect an EPVS to a variable DC load, and the boost's converter specs are illustrated in Table 3. The block for generating PWM signals from the duty ratio values is given in Figure 5(b). The two sensors for measuring voltage and current are Cleqee A622 and TA057, respectively. The sensors have been connected to the dSPACE acquisition board through the ADC ports. The measurements of the sensors have been filtered with digital filters implemented on the dSPACE board, as can be seen through Figure 5(a). The experimental results in Figure 6 have been given at a varying load profile. The load variation was controlled from a dSPACE signal. Figure 5(a) shows the blocks providing the load variation. The observed voltage and current signals are rescaled using gain scales of 10 and 20, respectively. The sample step time in this study is set to 50 μs.

Elgar 5500, a programmable DC power supply, has been used to emulate the electrical characteristics of the PV panel. With the help of this panel emulation, it is possible to make up for the absence of the PV panel and simulate variations in the different profiles. A dSPACE DS1104 controller with a 50 μs sample period is utilized to create the PV panel Simulink model. The boost converter is controlled by the last via PWM signals with an 8 kHz switching frequency. A DAC output is used to create the analog signal (0-10 V range) needed to command the Elgar 5500 source. The practical properties of the EPVS, as determined by adjusting the power DC supply's output current, are shown in Figure 7

5.1. Optimized Fuzzy MPPT Controller Using dSPACE Implementation. As discussed in the introduction, the reason for implementing the fuzzy MPPT approach is to verify the proposed algorithm experimentally using a dSPACE control board. The fuzzy MPPT controller is computed and optimized under Matlab/Simulink. The control system is set up in accordance with the configuration described in Section 3.

Five membership functions are used to calculate the output variable (ΔD_N) for the FLC as well as the input variables (e and Δe)). The variation's ranges for Δe, e, and the output are [−50, 50], [−35, 5], and [−1.5, 1], respectively.

The dSPACE board is the appropriate hardware prototyping improvement solution for doing real-time simulations in many domains and prototyping high-speed digital controllers. These controllers use the MATLAB real-time interfacing toolbox to connect the SIMULINK model to the actual hardware models. Control desk software is used as an acquisition management tool to facilitate real-time analysis of system performance and visualization of PV output waveforms. It is simple to adjust the controller's settings, manage the output load, or change the PV panel's model's mimicked weather patterns using the control desk software. The obtained currents and voltages may also be easily stored and displayed. The main points in the fuzzy MPPT-GA designing in this article are as follows:

(1) GA learning algorithm
(2) Experimental testing results

5.1.1. GA's Learning Profile. It is important to note that the optimal parameters of the fuzzy MPPT controller obtained by the GA are strongly related to the adopted methodology. The richer the learning profile and the more real variations in atmospheric conditions are taken into account, the higher the performance of the GA should be. At each step of the algorithm, we have to compromise between exploring the search space to avoid stagnating in a local optimum and exploiting the best individuals obtained to reach better values in the surroundings. If the individuals of a population are too similar, the following populations may become more and more homogeneous. In this case, the evolution of a population may be reduced to the evolution of a single dominant individual, thus reducing the exploration of the search space (premature convergence). In order to be able to efficiently search, it is, therefore, required to maintain a balance between the exploitation of the good solutions encountered and the exploration of unknown areas. An excess of exploitation can lead to a premature convergence (bogging down in a local optimum), just as an excess of exploration could lead to a quasi-random search (no convergence).

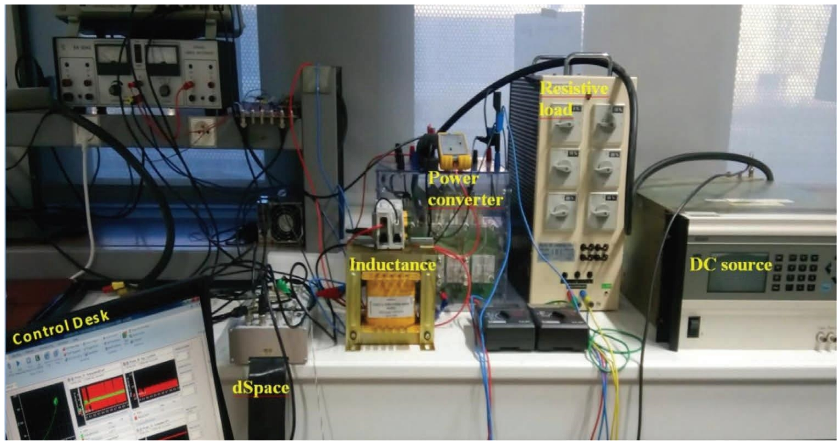

Figure 4: The experimental real-time platform.

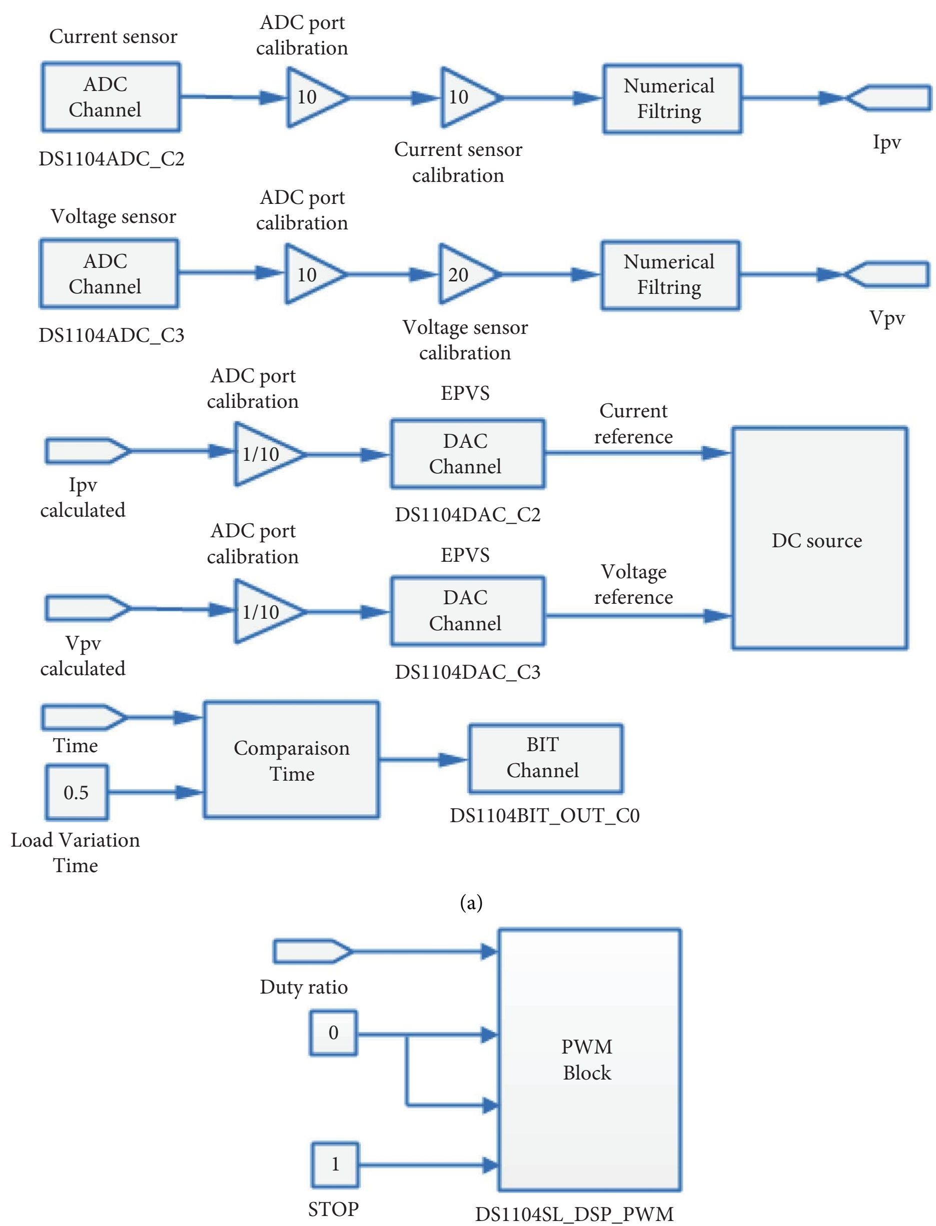

(a)

(b)

Figure 5: (a) ADC and DAC conversion blocks and (b) the PWM block.

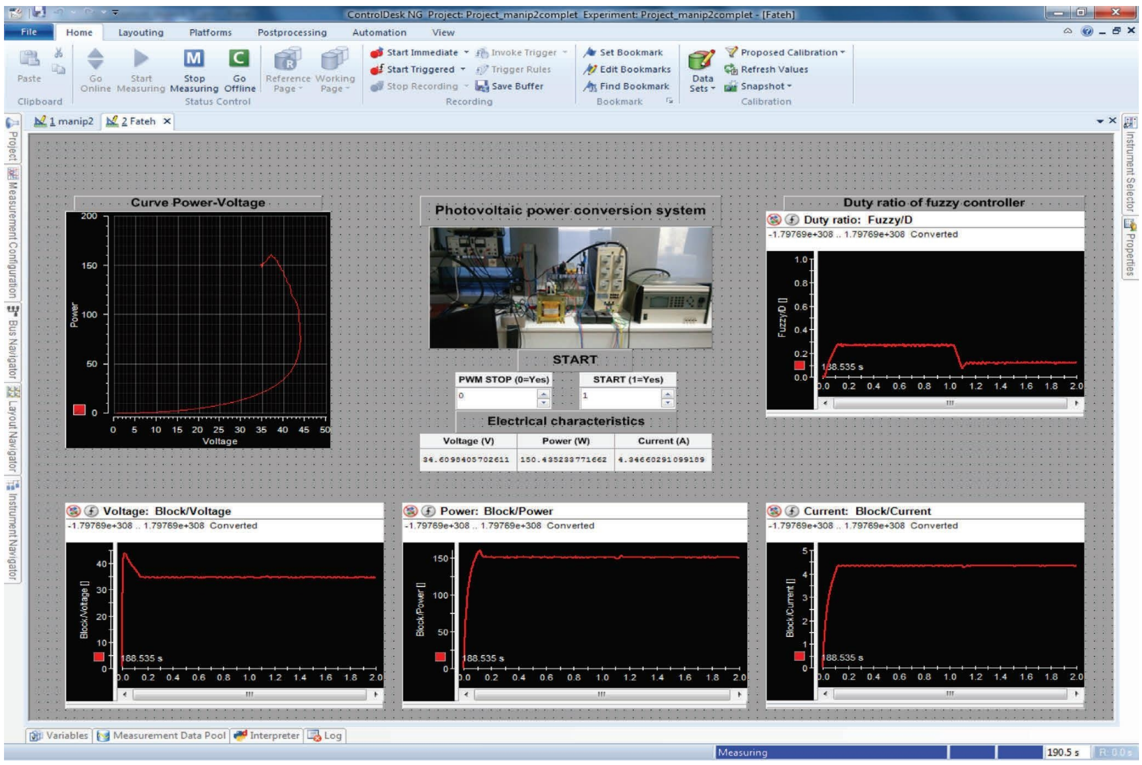

FIGURE 6: The control desk interface of the EPVS system.

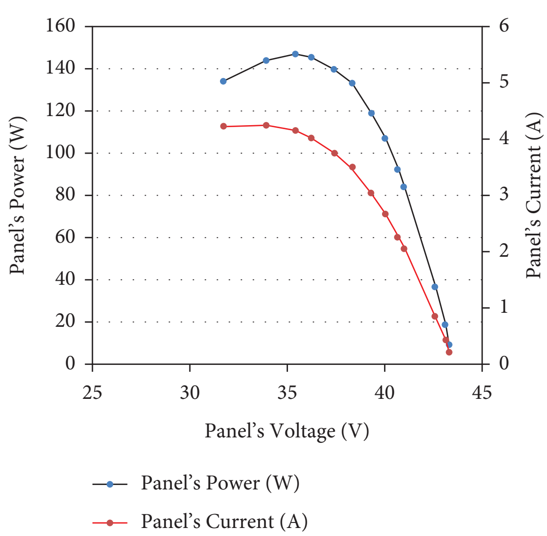

FIGURE 7: EPVS's experimental electrical characteristics.

The learning profile of the GA adopted is important for an optimal parameter result and must include any scenario that the system may encounter in the irradiance variations and from the values returned by the objective function ISE. A selection of the best chromosome (individuals) has been made by the algorithm. For this purpose, the parameters of the best chromosome were introduced to the fuzzy MPPT controller.

The value in the learning profile begins at 600 W/m^2 and changes at 1100 W/m^2 after 2 s; this value is maintained until 4 s after another change occurs to reach the value of 800 W/m^2.

The simulation results are given at a population of 20 chromosomes, and the training of the algorithm has been given at 200 iterations. The values of the fitness function ISE evolve in a decreasing way from iteration 01 to iteration 50. Beyond this iteration, the evolution of the curve is constant until it reaches the value ISE 0.372. The fact of training the algorithm beyond 50 iterations tells us that the algorithm has found a global optimum. The evolution of the ISE function curve per iteration is shown in Figure 8.

5.1.2. Experiments Testing Results. After the learning process is accomplished, we can see the tracking performance corresponding to the optimal solution obtained by the GA. The experimental testing results are obtained using the following two scenarios. The studied EPVS system has been evaluated in a 2 s total duration with a 50 μs fixed step size during the testing phases.

(i) In the first test, the solar irradiance and temperature are kept constant at STC conditions, but an instantaneous load change is performed at 1s. The resistance goes from a value of 20 Ω to 14 Ω.

(ii) In the second test, the load is kept constant at $R = 20\ \Omega$. However, the goal of this test is to study the impact of the fast-changing of solar irradiance on the performance of the proposed MPPT algorithm.

(1) Performance Test at Standard Conditions and Fast Varying Load Conditions. An interface controls the

parameters of the experimental test bench of the EPVS system and thus displays the curves and results of the electrical characteristics. The control of parameters is given by two buttons: START and PWM STOP. In order to activate the control part, the START value is set to 1, and the PWM STOP value is set to 0. The values of the electrical characteristics represented are voltage (V), power (W), and current (A). The curves shown are the power-voltage curve, the duty cycle of the proposed controller, and thus the voltage, power, and current.

The results represented in this interface have been given for a temperature of 25°C and sunshine 1000 W/m^2 as well as a fast-varying resistance load. Figure 6 shows the control desk interface of the EPVS system.

Figures 6 and 9 show the results of the generated EPVS power of the proposed fuzzy MPPT-GA. In the presented results, during the transient load step of $R = 20\,\Omega$ between 0 s and 0.5 s, it can be seen that the proposed fuzzy MPPT-GA converges rapidly to the MPP at a time of 0.08 s with a tracking error of 3% and a steady state-error of 99.87% and then the power is maintained around 150 W with an extremely low steady-state error of about ±0.13%. The total error between the tracking error and the steady-state error is about 96.87%.

In the second transient load step of $R = 14\,\Omega$ between 0.5 s and 1 s, it is clearly observed that the proposed fuzzy MPPT-GA shows better power generation, which much perfectly rated around 150 W with an extremely low steady-state error of about ±0.13% (99.87%) as depicted in Figures 6 and 9. It can be concluded that the proposed fuzzy MPPT-GA completely follows the maximum power of 150 W to the STC test profile and also to the fast-varying load conditions.

Figure 10 shows the result of the duty ratio of the proposed fuzzy MPPT-GA at the STC. It can be observed a variation in the duty ratio value as soon as 0.5 s. In the presented results, during the transient load step of $R = 20\,\Omega$ between 0 s and 0.5 s, it can be seen that the proposed fuzzy MPPT-GA generates a duty ratio of the value $D = 0.25$. It is evident that the proposed fuzzy MPPT-GA generates the corresponding new duty ratio D ($D = 0.15$) for each transaction period in the second transient load level of $R = 14\,\Omega$ between 1 s and 2 s, which establishes the new position of the desired MPP inversely. In this case, the duty ratio of the proposed fuzzy MPPT-GA is optimally adjusted. It is clearly shown that a perfect duty ratio is generated in order to keep the power produced at its desired value.

(2) Performance Test under Fast-Changing Solar Irradiation. The test at standard conditions, as well as at the fast variation of the load, has been successfully performed. Now, a test at fast variation solar irradiation has been performed. The load was held fixed at $R = 20\,\Omega$. The choice of the value between $R = 20\,\Omega$ or $R = 14\,\Omega$ is not important since the result given in Figures 6 and 9 clearly shows that the power is maintained at 150 W with an error of 0.13% at the static regime for both the resistance values.

Figure 11 shows the irradiance profile, which varies between 1000 W/m^2 and 1100 W/m^2, and both the temperature and the load charge are kept constant during the experiments at 25°C and $R = 20\,\Omega$, respectively.

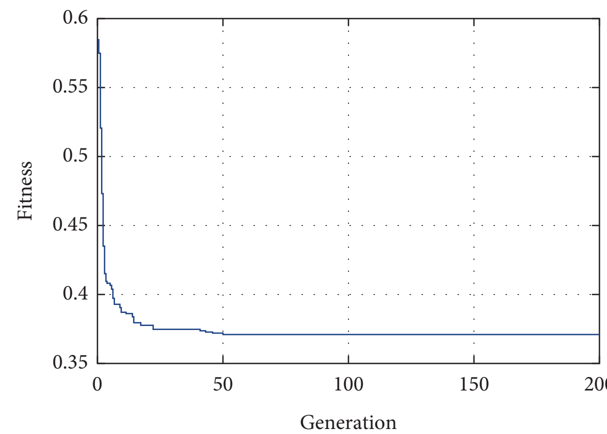

FIGURE 8: Evolution of the fitness function curve.

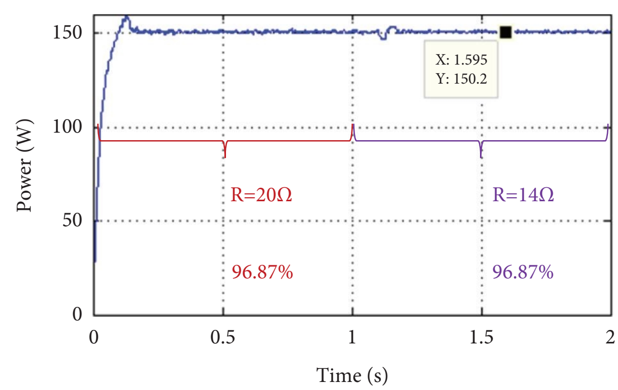

FIGURE 9: The experimental result of PV power under STC and fast-varying load.

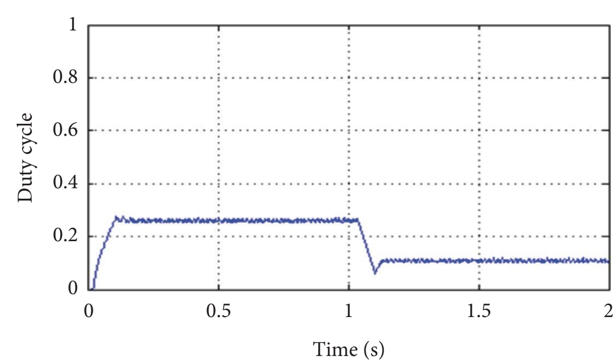

FIGURE 10: The experimental result of the duty ratio ΔD_N under STC and fast-varying load.

The experimental performance test has been carried out at the fixed charge 20 Ω and the fast-changing solar irradiance, as shown in Figure 11. In this test case, the objective has been to evaluate and observe the response of the proposed fuzzy MPPT-GA only to the fast-changing solar irradiance and at the constant ambient temperature 25°C.

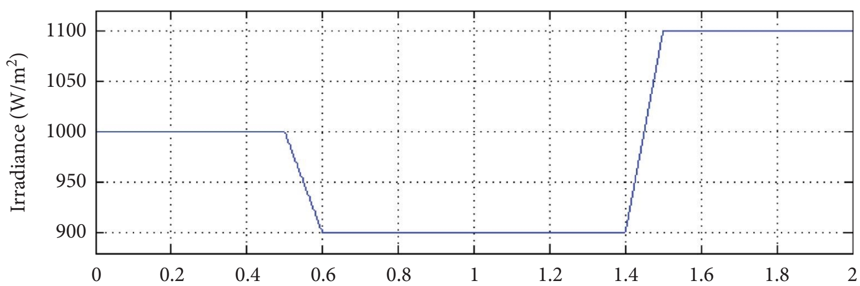

FIGURE 11: The irradiance profile.

Figure 12 shows the results of the generated EPVS power of the proposed fuzzy MPPT-GA. In the presented results, during the transient irradiance value between 0 s and 0.5 s, it can be seen that the proposed fuzzy MPPT-GA converges very rapidly to the MPP at a time of 0.06 s with a tracking error of 2.6% and a steady-state error of 99.85% and then the power is maintained around 150 W for a 1000 W/m^2 with an extremely low steady-state error of about ±0.10%. The total error between the tracking error and the steady-state error is about 97.25%. In the second step, the transient irradiance value is between 0.5 s and 1.4 s. It can be seen that the proposed fuzzy MPPT-GA also converges at the MPP with an extremely low steady-state error of about ±0.12% (99.82%). In the last step, during the transient period of 1.4 s to 2 s, it can be seen that the proposed fuzzy MPPT-GA also converges at the MPP with an extremely low steady-state error of about ±0.14% (99.79%). The efficiency of the EPVS system in the three transient irradiance values has been given at 98.95%. It can be clearly observed that the result, when the MPP abruptly changes, is that the proposed fuzzy MPPT-GA may immediately push the EPVS system to the new MPP.

Figure 13 shows the result of the duty ratio of the proposed fuzzy MPPT-GA under fast-changing solar irradiation. It can be clearly observed that a new value of the duty cycle has been generated at each variation of the irradiance. In this case, the duty ratio of the proposed fuzzy MPPT-GA has been optimally adjusted in order to keep the operating point at each instant at the MPP.

Now, the proposed fuzzy MPPT-GA has been compared with a few strategies which have been published in recent works to optimize FLC-based MPPT meths. Authors in [18, 24, and 25] have performed the performance tests of standalone PV systems only at STC conditions with a fixed resistance load. The results of tests for a profile of variable irradiance that present overshoots when changing the values of irradiance more or less different from one paper to another have been presented in [18, 19, and 21].

For a more logical comparison, the optimization algorithms should use the same objective function (equation (7)), the same initial population, and also the same number of iterations. The advantages of our design strategy, which provides the best objective function (ISE) value at the conclusion of the optimization process, have been shown in Figure 8.

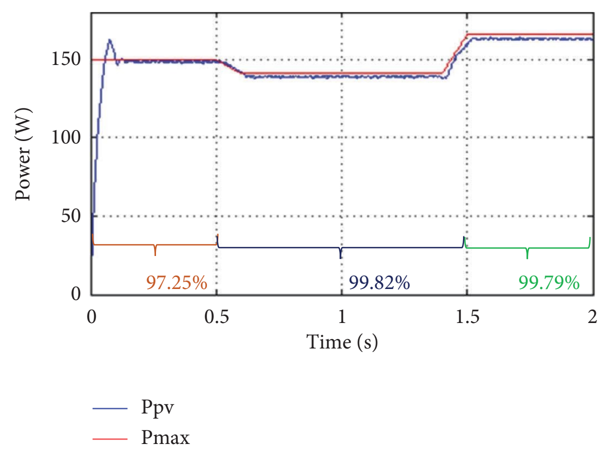

FIGURE 12: The experimental result of PV power under fast-changing solar irradiation.

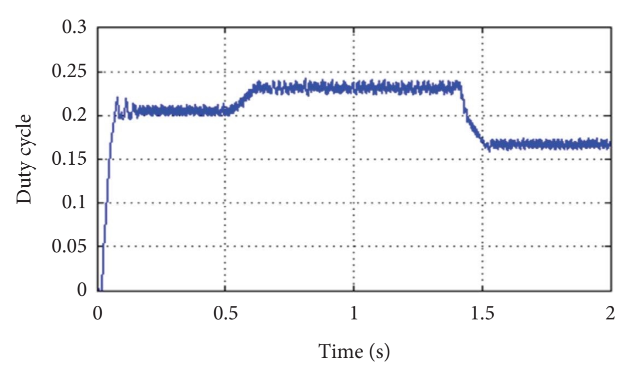

FIGURE 13: The experimental result of the duty ratio ΔD_N under fast-changing solar irradiation.

6. Conclusion

This paper presents a modeling and experimental validation of a standalone PV system. The system under investigation consists of a DC power source that simulates a solar panel, a DC/DC boost converter, a resistive load, and a real-time maximum power point tracking controller integrated into a dSPACE DS1104 board. The GA has been successfully applied in this study to optimize the productivity of a fuzzy MPPT algorithm by improving the controller's membership function parameters. From the objective function values obtained in the simulation, it is seen that the GA provides a good approach for designing efficient fuzzy MPPT. The following are the main highlights of the current work:

(i) The proposed GA algorithm's learning profile was extremely important. The results obtained during the tests using the various profiles clearly show that the parameters of the fuzzy controller's input/output membership functions determined during the optimization process accurately follow the GMPP with a steady-state error of around ±0.13%.

(ii) Similar to that, a reference signal has been used to compare the proposed approach. The outcomes demonstrated the suggested algorithm's capability to track the GMPP with quicker convergence and fewer power fluctuations than before. The suggested fuzzy controller optimized-based MPPT's viability and efficacy have been tested experimentally, and the findings unmistakably show that it is capable of tracking the GMPP with an average efficiency of 98.66% and an average tracking time of 0.08 s and 0.06 s under the STC and the fast-changing solar irradiance, respectively.

The outcomes demonstrated that the suggested approach was workable and that it was capable of tracking the maximal power point with high efficiency that exceeded 97.8% in all tested scenarios. The method proposed has been described in some detail and can be used in other similar systems.

Data Availability

The data supporting the findings of the current study are available from the corresponding author upon request.

Conflicts of Interest

The authors declare that they have no conflicts of interest.

References

[1] S. S. Kshatri, J. Dhillon, S. Mishra et al., "Reliability analysis of bifacial PV panel-based inverters considering the effect of geographical location," *Energies*, vol. 15, p. 170, 2021.

[2] M. U. Siddiqui, O. K. Siddiqui, A. B. Alquaity, H. Ali, A. F. M. Arif, and S. M. Zubair, "A Comprehensive Review on Multi-Physics Modeling of Photovoltaic Modules," *Energy Conversion and Management*, Article ID 115414, 2022.

[3] N. M. Kumar, S. Islam, A. K. Podder, A. Selim, M. Bajaj, and S. Kamel, "Lifecycle-based feasibility indicators for floating solar photovoltaic plants along with implementable energy enhancement strategies and framework-driven assessment approaches leading to advancements in the simulation tool," *Frontiers in Energy Research*, vol. 11, 2023.

[4] C. Aoughlis, A. Belkaid, I. Colak, O. Guenounou, and M. A. Kacimi, "Automatic and self-adaptive P&O MPPT based PID controller and PSO algorithm," in *Proceedings of the 2021 10th International Conference on Renewable Energy Research and Application (ICRERA)*, pp. 385–390, IEEE, Istanbul, Turkey, September 2021.

[5] R. Kumar, S. Khandelwal, P. Upadhyay, and S. Pulipaka, "Global maximum power point tracking using variable sampling time and pv curve region shifting technique along with incremental conductance for partially shaded photovoltaic systems," *Solar Energy*, vol. 189, pp. 151–178, 2019.

[6] F. Zaouche, D. Rekioua, J. P. Gaubert, and Z. Mokrani, "Supervision and control strategy for photovoltaic generators with battery storage," *International Journal of Hydrogen Energy*, vol. 42, no. 30, pp. 19536–19555, 2017.

[7] M. Sarvi and A. Azadian, "A comprehensive review and classified comparison of MPPT algorithms in PV systems," *Energy Systems*, vol. 13, no. 2, pp. 281–320, 2021.

[8] F. Yahiaoui, F. Chabour, O. Guenounou et al., "Experimental validation and intelligent control of a stand-alone solar energy conversion system using dSPACE platform," *Frontiers in Energy Research*, vol. 10, 2022.

[9] D. Rekioua, F. Zaouche, H. Hassani, T. Rekioua, and S. Bacha, "Modeling and fuzzy logic control of a stand-alone photovoltaic system with battery storage," *Turkish Journal of Electromechanics and Energy*, vol. 4, no. 1, 2019.

[10] A. Boudia, S. Messalti, A. Harrag, and M. Boukhnifer, "New hybrid photovoltaic system connected to superconducting magnetic energy storage controlled by PID-fuzzy controller," *Energy Conversion and Management*, vol. 244, Article ID 114435, 2021.

[11] C. Balasundar, S. Ck, S. Ns, and J. M. Guerrero, "Interval type-II fuzzy logic controlled shunt converter coupled novel high-quality charging scheme for electric vehicles," *IEEE Transactions on Industrial Informatics*, 2020.

[12] A. Mohammadzadeh, M. H. Sabzalian, and W. Zhang, "An interval type-3 fuzzy system and a new online fractional-order learning algorithm: theory and practice," *IEEE Transactions on Fuzzy Systems*, vol. 28, no. 9, pp. 1940–1950, 2020.

[13] D. S. Abraham, B. Chandrasekar, N. Rajamanickam et al., "Fuzzy-based efficient control of DC microgrid configuration for PV-energized EV charging station," *Energies*, vol. 16, no. 6, p. 2753, 2023.

[14] A. Jaiswal, Y. Belkhier, S. Chandra et al., "Design and implementation of energy reshaping based fuzzy logic control for optimal power extraction of PMSG wind energy converter," *Frontiers in Energy Research*, vol. 10, 2022.

[15] S. B. Hamed, A. Abid, M. B. Hamed et al., "A robust MPPT approach based on first-order sliding mode for triple-junction photovoltaic power system supplying electric vehicle," *Energy Reports*, vol. 9, no. 2023, pp. 4275–4297, 2023.

[16] D. E. Goldenberg, "Genetic Algorithms in Search," *Optimization and Machine Learning*, 1989.

[17] A. Hadjaissa, S. Ait cheikh, K. Ameur, and N. Essounbouli, "A GA-based optimization of a fuzzy-based MPPT controller for a photovoltaic pumping system, Case study for Laghouat, Algeria," *IFAC-PapersOnLine*, vol. 49, no. 12, pp. 692–697, 2016.

[18] A. Borni, T. Abdelkrim, N. Bouarroudj et al., "Optimized MPPT controllers using GA for grid connected photovoltaic systems, comparative study," *Energy Procedia*, vol. 119, pp. 278–296, 2017.

[19] O. Guenounou, A. Belkaid, I. Colak, B. Dahhou, and F. Chabour, "Optimization of fuzzy logic controller based maximum power point tracking using hierarchical genetic algorithms," in *Proceedings of the 2021 9th International Conference on Smart Grid (icSmartGrid*, pp. 207–211, IEEE, Setubal, Portugal, June 2021.

[20] K. Loukil, H. Abbes, H. Abid, M. Abid, and A. Toumi, "Design and implementation of reconfigurable MPPT fuzzy controller for photovoltaic systems," *Ain Shams Engineering Journal*, vol. 11, no. 2, pp. 319–328, 2020.

[21] A. Messai, A. Mellit, A. Guessoum, and S. A. Kalogirou, "Maximum power point tracking using a GA optimized fuzzy logic controller and its FPGA implementation," *Solar Energy*, vol. 85, no. 2, pp. 265–277, 2011.

[22] C. N. S. Kalyan, B. S. Goud, M. Bajaj, M. K. Kumar, E. M. Ahmed, and S. Kamel, "Water-cycle-algorithm-tuned intelligent fuzzy controller for stability of multi-area multi-fuel power system with time delays," *Mathematics*, vol. 10, no. 3, p. 508, 2022.

[23] A. Youssef, M. E. Telbany, and A. Zekry, "Reconfigurable generic FPGA implementation of fuzzy logic controller for MPPT of PV systems," *Renewable and Sustainable Energy Reviews*, vol. 82, pp. 1313–1319, 2018.

[24] A. Ilyas, M. R. Khan, and M. Ayyub, "FPGA based real-time implementation of fuzzy logic controller for maximum power point tracking of solar photovoltaic system," *Optik*, vol. 213, Article ID 164668, 2020.

[25] S. Hadji, J. P. Gaubert, and F. Krim, "Real-time genetic algorithms-based MPPT: study and comparison (theoretical an experimental) with conventional methods," *Energies*, vol. 11, no. 2, p. 459, 2018.

[26] D. Fares, M. Fathi, I. Shams, and S. Mekhilef, "A novel global MPPT technique based on squirrel search algorithm for PV module under partial shading conditions," *Energy Conversion and Management*, vol. 230, Article ID 113773, 2021.

[27] I. Shams, S. Mekhilef, and K. S. Tey, "Maximum power point tracking using modified butterfly optimization algorithm for partial shading, uniform shading, and fast varying load conditions," *IEEE Transactions on Power Electronics*, vol. 36, no. 5, pp. 5569–5581, 2021.

[28] M. B. Yaouba, M. Bajaj, C. Welba et al., "An experimental and case study on the evaluation of the partial shading impact on PV module performance operating under the sudano-sahelian climate of Cameroon," *Frontiers in Energy Research*, vol. 10, 2022.

[29] R. Khelifi, M. Guermoui, A. Rabehi et al., "Short-term PV power forecasting using a hybrid TVF-EMD-ELM strategy," *International Transactions on Electrical Energy Systems*, vol. 2023, Article ID 6413716, 14 pages, 2023.

[30] X. Weng, X. Xiao, W. He et al., "Comprehensive comparison and analysis of non-inverting buck boost and conventional buck boost converters," *Journal of Engineering*, vol. 2019, no. 16, pp. 3030–3034, 2019.

[31] S. Tamalouzt, Y. Belkhier, Y. Sahri, N. Ullah, R. N. Shaw, and M. Bajaj, "New direct reactive power control based fuzzy and modulated hysteresis method for micro-grid applications under real wind speed," *Energy Sources, Part A: Recovery, Utilization, and Environmental Effects*, vol. 44, no. 2, pp. 4862–4887, 2022.

[32] O. Guenounou, B. Dahhou, and F. Chabour, "TSK fuzzy model with minimal parameters," *Applied Soft Computing*, vol. 30, pp. 748–757, 2015.

[33] L. Brikh, O. Guenounou, and T. Bakir, "Selection of minimum rules from a fuzzy TSK model using a PSO–fcm combination," *Journal of Control, Automation and Electrical Systems*, vol. 34, no. 2, pp. 384–393, 2022.

Hindawi
Mathematical Problems in Engineering
Volume 2023, Article ID 2691439, 16 pages
https://doi.org/10.1155/2023/2691439

Research Article

Intelligent System for Optimal Geometric Design Using Fuzzy Soft PDE

Nosshad Jamil,[1] **Syed Kirmani**,[1] **Shakrullah Wadeer**,[2] **and Alqa Sultanl**[1]

[1]*University of Management and Technology, Lahore, Pakistan*
[2]*Nangarhar University, Kabul-Jalalabad Highway, Daronta, Nangarhar, Afghanistan*

Correspondence should be addressed to Shakrullah Wadeer; shukrullah.umt21@gmail.com

Received 17 October 2022; Revised 22 January 2023; Accepted 6 April 2023; Published 26 April 2023

Academic Editor: Arunava Majumder

In this research, a methodology is discussed to develop an intelligent system for optimal geometric design for the culinary product. An optimum geometric design meets certain specified criteria in the most efficient or cost-effective way possible. The criterion for an optimum design will depend on the specific goals and constraints of the specific problem. In this methodology, partial differential equation and weighted Bonferroni mean are consolidated to develop the intelligent system for optimal geometric designs for the required product with the blend of fuzzy soft sets. Fuzzy soft sets allow capturing the incorporation of subjective or personal opinions into decision-making processes, as well as the consideration of multiple conflicting criteria. A parameter known as the smoothness parameter is used to control the shape of the optimal geometric model. The smoothness parameter, used as a fuzzy number, is important in this developed system as it fulfills the requirements for the desired intelligent system for product design according to the industries' demands. To verify the credibility of this system, an illustrated example is presented to design a culinary product, which is profitable for the hotel industry.

1. Introduction

Computer-aided design (CAD) is a technique discussed by Sarcar et al. in [1]. This technique is used in the creation, modification, analysis, and optimization of the geometric modeling of products with the help of computers. As mentioned in [2], the fewer number of design variables and the intuitive control of the design for the user are the key aspects of efficiency in systems used for the mathematical modeling of three-dimensional surfaces. Surface modeling, solid modeling, and particle system modeling are the different types of three-dimensional modeling discussed in [3].

Authors discussed in [4], when one surface patch of a set of patches is varied, it creates difficult situations such as maintaining the smooth continuity of the shape. According to Frey and Borouchaki in [5], a surface can be defined geometrically by moving a line in space in a direction other than the line itself. The surface under consideration can be defined as the area swept by the movement. If either the line or the movement is curved, the resulting surface is curved. The direction of the line is known as the g direction in mathematics, and the direction of movement of the line is known as the h direction. The h parameter notation is crucial in CAD concepts and plays an important role in generating surfaces as discussed in [6]. Patches are classified based on the shape of their originating curves. As mentioned in [7], Bezier splines produce a Bezier patch, and two B-spline curves produce a B-spline patch, as discussed in [8]. A patch will inherit features such as control points from its original spline curves. As a result, the number and position of a patch's control points are determined by the control points associated with each of the spline curves. These control points can be used to modify the patch in the same way that control points can be used to manipulate a curve.

The smoothness and extendibility of the surface's topology are the two most important issues in the computer modeling of surfaces. As mentioned in [9], patches, which are mathematically truly curved, are the solution for smooth surfaces. They must, however, be constructed with grid-like rows and columns. According to the author's explanation in

[10], surfaces are subdivided to make them smooth. To achieve the smooth curvature of the surface, the simple polygonal model is subdivided into smaller polygons in this technique. The extent to which the original polygons are subdivided is determined by the curvature of the end surface. When a curve or surface is infinitely subdivided, the result is truly curved and is known as a limit curve or limit surface as discussed in [11]. The most important aspect of the subdivision technique is that it allows to manipulate the shape of the model with both the original polygonal model and the subdivision model. When the original polygonal model is used, the subdivision result is also modified. Moreover, if the subdivision model is manipulated, the changes will have no effect on the original polygon model.

The surface generation method based on partial differential equations, mentioned in [12], is another efficient mathematical model for representing real-world objects that addresses some of the drawbacks discussed in the preceding methods. It is particularly appealing due to the fact that it allows for intuitive manipulation of the shape of the object with minimal user interaction. With a slight change in its design parameters, it generates a wide range of shapes from a single equation. This technique, also known as the PDE method discussed in [13, 14], entails solving a suitable partial differential equation over a set of boundary conditions. A design parameter is also included in the equation to give the user more flexibility in changing the shape of the object with less effort. This method's rendering process is also simple, as it entails solving a mathematical equation to generate points and plot them to create the desired surfaces and shapes. Patches of the surfaces generated by this method can be used to create objects with complex shapes.

According to Ugail and Wilson in [14, 15], geometric modeling, using the spline approach for design optimization, has the disadvantage of making it difficult to maintain a smooth transition between adjacent patches during the design process. It happens because they typically represent an object shape as a mesh of rectangular curvilinear parts. The parameterizations of a product's shape are considered relatively simple if it is made up of standard geometric constructs such as circles, squares, cubes, and cylinders. However, in general, most products cannot be completely constructed using these standard shapes alone but must also include free form surfaces in their design to achieve the desired shape. Regardless of how minor these surfaces are in the overall shape of the object, they may be critical if they are part of the object's functionality. It should be noted that the PDE method is similar in some ways to previously established surface design methods such as Bezier patches and rational B-splines discussed in [15–18]. However, PDE's global smoothing approach, in conjunction with its elliptic boundary-value formulation, clearly distinguishes it from those traditional spline-based techniques. When compared to the hundreds of control points required by existing spline-based techniques, PDE requires only a small set of design variables. As mentioned in [19], Ugail et al. research in the area of interactive design demonstrated that PDE surfaces could be defined and manipulated efficiently in real time. Authors also demonstrated that surface manipulation could be performed in an interactive environment with an interactively defined set of parameters, discussed in [19–22]. These parameters, by definition, make their effect on the geometry of the surface obvious.

Regarding interactive design using the PDE method, Bloor and Wilson showed in [23] that, this method can produce simple surfaces in an interactive environment. This work was then extended by Ugail et al., mentioned in [19, 20]. They used four boundary conditions in the PDE method to generate surface. Later, their work was extended by Ugail et al., discussed in [24], in which they used six boundary conditions to generate the geometric surface. It was easier to work with six boundary conditions than with four boundary conditions, as a more curvier geometric model can be generated and a complex geometric model can be generated more easily. In this article, their work is further extended by using eight boundary conditions to develop the complex geometric model with the help of a set of interactively defined parameters. The boundary conditions are responsible to control the overall form of the surface of the designed model, while a set of parameters control all the coordinates of the boundary conditions. One of the parameters involved in the designing of the desired model is the modified smoothness parameter, responsible for the smoothness and quality of the geometric model, which is developed with the help of the fuzzy soft matrix (FSM) along with weighted Bonferroni mean (WBM).

The fuzzy soft matrix (FSM) is a very useful tool to gather requirements of the industry for designing their products, while weighted Bonferroni mean (WBM) blend the requirements of industry into a single entity. According to Zadeh discussed in [25], fuzzy sets theory is useful for modeling uncertain circumstances better than standard theories. In 1999, Molodtsov introduced the concept of soft set, discussed in [26], and successfully solved some uncertainties. Later, Maji et al. [27] modified the concept of soft set theory and successfully applied it to decision-making problems. In 2001, Maji et al. in [28] presented the concept of the fuzzy soft set by combining the concept of the fuzzy set with the soft set. One of the main advantages of fuzzy soft sets is that they allow for the incorporation of subjective or personal opinions into decision-making processes, as well as the consideration of multiple conflicting criteria. This can be particularly useful in situations where there is a lack of objective data or where multiple stakeholders have different viewpoints or priorities.

Fuzzy soft sets have been applied in a wide range of fields, including decision analysis, artificial intelligence, information retrieval, and control systems. They are often used in conjunction with other techniques, such as fuzzy logic or artificial neural networks, to improve the accuracy and robustness of decision-making systems. This theory opened the path to many new concepts. Neog and Sut mentioned in [29] used fuzzy soft complement and fuzzy soft matrix operation to solve decision-making problems. Sut in [30] utilizes fuzzy soft relations in a decision-making problem.

Cagman et al. in [31] proposed a decision-making method that makes use of a fuzzy soft aggregation operator and a cardinal set. Celik and Yamak in [32] used fuzzy soft set theory with a fuzzy aggregation operator to diagnose patients' diseases. In 2018, Beg et al. [33] developed a time-dependent model to analyse human attributes by fuzzy soft matrix (FSM) and Bonferroni mean (BM). BM was developed by Bonferroni in [34], which was helpful in the multiple comparison test. Yager in [35, 36] and Beliakov et al. in [37] discussed useful properties of BM to capture the interrelationships among arguments. Using the concept of BM with fuzzy soft matrix, Beg et al. explained in [33] and defined Bonferroni fuzzy soft matrix (BFSM) and weighted Bonferroni fuzzy soft matrix (WBFSM) for data representation. They also used WBFSM for design making.

An optimum geometric design is a design that meets certain specified criteria in the most efficient or cost-effective way possible. The criteria for an optimum design will depend on the specific goals and constraints of the problem at hand and may include factors such as strength, stiffness, weight, cost, and manufacturability.

In this article, the concept of WBFSM is used to calculate the modified smoothness parameter used in the partial differential equation. Since the requirements for designing an intelligent system to generate a geometric model for an industry can only be provided in the form of fuzzy soft set and single value is required for smoothness parameter, so this intelligent system was needed to convert fuzzy soft set in a single number. For this purpose, WBFSM is used in this article as it is an ideal tool to blend multiple values in a single value.

To verify this intelligent system, an example is taken from the hotel industry to design a drinking glass for fizzy drinks. According to a case study discussed in [38], drinking behavior of a person highly depends on the design of a glass. If the glass has an effective design and is easy to drink from, then the person will drink more than usual. The design of a glass also depends on the type of drinks. It is also discussed in the same case study, how design of glass affects the drinking behavior of a person. Considering the drinking behavior and the type of drink, it can be very helpful in designing a glass. In the making of a drinking glass, many parameters are considered (such as quality, material used in glass, and price) according to the requirement of the customer. But the problem is that a customer is not able to see it until the manufacturing of the glass is complete. Sometimes, the final result is not according to the customer's requirement. For this purpose, a three-dimensional design of a drinking glass according to the required parameters is generated. The intelligent system developed in this article is used to generate multiple designs of drinking glass according to customer's requirements. After modeling these designs, multicriteria decision-making (MCDM) is used to select the glass which efficiently fulfills the customer requirements.

The structure of this article is as follows: Section 2 is devoted, the basic definitions used in this research, which will help the reader in understanding this research. Section 3 provides the detail on the PDE used in this research along with some geometric models generated using the involved PDE method. In Section 4, forming of the smoothness parameter with the help of WBFSM is discussed in detail. In this section, we also developed an intelligent system and with the help of illustrated examples, we verified the credibility of the developed system. Finally, the last section of this article is concluded with the discussion on the benefits and utilization of the developed system in different designing industries. A path for further research is also mentioned in this section.

2. Preliminaries

Partial differential equation (PDE) is a tool which is used in every field of mathematics. In this article, a hybrid methodology is developed by using fuzzy sets and soft sets theory with blend of eighth order PDE with some boundary conditions and a set of parameters. In this chapter, some basic definitions are discussed which will be helpful in further discussion.

Definition 1 [25]. Let X be a nonempty set. A fuzzy set A in X is characterized by its membership function $\mu_A\colon X \longrightarrow [0,1]$, and $\mu_A(X)$ is interpreted as the degree of membership of element x in the fuzzy set A for each $x \in X$.

Definition 2 [26]. Let Y be a universal set, E be a set of parameters, and A be a subset of E. Power set of Y is denoted by $P(Y)$, then the pair $(F;A)$ is said to be a soft set over the universal set Y, where F is mapping given by $F\colon A \longrightarrow P(Y)$. In fact, a soft set is a parameterized family of subsets over the universal set Y . Every set $(F(e);e)$ represents the set of elements of the soft set $(F;A)$.

Definition 3 [39]. If Y be the universal set, E be the set of parameters, and $B \subseteq E$ and P^Y be the set of all fuzzy subsets of Y, then (G,B) is said to be the fuzzy soft set over Y, where G is a mapping such that $G\colon B \longrightarrow P^Y$. Tabular representation of a fuzzy soft set is represented in Table 1.

Definition 4 [37]. Let there be two natural numbers s,t and $r_i \geq 0$ for $(i = 1,2,\cdots,n)$. Then, Bonferroni mean $F^{s,t}$ is as follows:

$$F^{s,t} = \left(\frac{1}{n(n-1)} \sum_{i,j=1, i\neq j}^{n} r_i^s r_j^t\right)^{(1/s+t)}. \tag{1}$$

The Bonferroni mean (BM) is a useful aggregative operator that is an extension of the arithmetic mean. The Bonferroni mean (BM) has the property of capturing the interrelationships between factors that are significant for multicriteria decision-making, according to Yager [35]. The following scenario for BM was studied by Dyckhoff and Pedrycz [40] for various s and t values.

(i) If $s = 1$ and $t = 0$, then

$$F^{1,0} = \left(\frac{1}{n} \sum_{i=1}^{n} r_i\right). \tag{2}$$

(ii) If $s = 2$ and $t = 0$, then

Table 1: Tabular representation of a fuzzy soft set (G, B).

	y_1	y_2	y_3	$\cdots$	y_n
e_1	a_{11}	a_{12}	a_{13}	$\cdots$	a_{1n}
e_2	a_{21}	a_{22}	a_{23}	$\cdots$	a_{2n}
e_3	a_{31}	a_{32}	a_{33}	$\cdots$	a_{3n}
.	.	.	.	.	.
.	.	.	.	.	.
.	.	.	.	.	.
e_m	a_{m1}	a_{m2}	a_{m3}	$\cdots$	a_{mn}

$$F^{2,0} = \left(\frac{1}{n}\sum_{i=1}^{n} r_i\right)^{(1/2)}. \tag{3}$$

(iii) If $s \longrightarrow +\infty$ and $t = 0$, then

$$\lim_{s \longrightarrow +\infty} F^{s,0} = \max_i \{r_i\}. \tag{4}$$

(iv) If $s \longrightarrow 0$ and $t = 0$, then

$$\lim_{s \longrightarrow 0} F^{s,0} = \left(\prod_{i=1}^{n} r_i\right)^{(1/n)}. \tag{5}$$

(v) If $s = 1$ and $t = 1$, then

$$F^{1,1} = \left(\frac{1}{n(n-1)}\sum_{i,j=1, i\neq j}^{n} r_i r_j\right)^{(1/2)}. \tag{6}$$

In equation (6), the operator's interpretation is a combination of the relational operators "and" and "average." Product activities, in particular, can be leveraged to implement two satisfaction requirements. As a result, r_i and r_j denote the degree to which the two requirements are satisfied. As a result, $F^{1,1}(r_1, r_2, \cdots r_n)$ estimates the reference pair's average satisfaction.

Definition 5 [35]. If s and t are two natural numbers and $r_i \geq 0$ for all $(i = 1, 2, 3, \cdots, n)$ and for any weighted vector $W = (w^i \geq 0)^T$ of r_i, which has condition $\sum_{i=1}^{n} w_i = 1$, then weighted Bonferroni mean is

$$WF^{s,t} = \left(\frac{1}{n(n-1)}\sum_{i,j=1, i\neq j}^{n} (w_i r_i)^s (w_j r_j)^t\right)^{(1/s+t)}. \tag{7}$$

Definition 6 [33]. Let there be a fuzzy soft matrix $F^h_{mn} = [f^h_{ij}]$ where $i = 1, 2, \cdots, m$, $j = 1, 2, \cdots, n$ and $h = 1, 2, \cdots, q$. Then, Bonferroni fuzzy soft matrix (BFSM) is defined as $F_{mn} = [f_{mn}]$, where $f_{mn} = F^{s,t}(f^1_{mn}, f^2_{mn}, \ldots, f^q_{mn})$. Here, s and t are natural numbers.

Definition 7 [33]. Let a fuzzy soft matrix be $F_{m\times n} = [f_{i,j}]$, where $i = 1, 2, \cdots, m$ and $j = 1, 2, \cdots, n$. Then, weighted Bonferroni fuzzy soft matrix (WBFSM) is defined as $F_{m\times 1} = [d_{i,1}]$ for weight vector $W = w_j$, which is the weight of $f_{i,j}$. The weight vector has the condition $\sum_j^n w_j = 1$. Here, $d_{i,1} = WF^{s,t}(f_{i,1}, f_{i,2}, \ldots, f_{i,n})$.

Definition 8 [33]. Optimum fuzzy soft constant (OFSC) is Optimum $= \max_i (c_{i,1})$, where $c_{i,1}$ is from the last definition.

2.1. Partial Differential Equation Surfaces. Wood ward introduced in [41] that the PDE method mainly aims to provide a skillful function accepting some specific boundary and continuity conditions, and this function works as a connecting surface for primary neighboring surfaces. Follow that a second order elliptic PDE method was used by Bloor and Wilson [42] to generate blend surfaces in the field of CAGD. They then extended their work and generated PDE surfaces using fourth order PDE [19, 20], which used four boundary conditions to generate surfaces. In this article using their work as a reference, eight order PDE surfaces are generated using eight boundary conditions.

$$\left(\frac{\partial^2}{\partial\alpha^2} + \eta^2\frac{\partial^2}{\partial\beta^2}\right)^4 \Omega(\alpha, \beta) = 0, \tag{8}$$

where $\Omega(\alpha, \beta) = (x(\alpha, \beta), y(\alpha, \beta), z(\alpha, \beta))$ is a parametric function.

To preserve the shape of the surface, the selection of boundary conditions and parametric domain are essential for equation (8). Here, Ω is normally taken as a rectangle, that is, Ω: $\alpha_0 \leq \alpha \leq \alpha_1, \beta_0 \leq \beta \leq \beta_1$. The parameter η is known as a smoothness parameter which plays an important role for the shape reconstruction of a model [41].

To solve the eighth order PDE, equation (8) required eight boundary conditions so that a unique solution in x, y, and z coordinates can be obtained. Due to this, in this research, the required PDE surface is generated by the solution of equation (8) with eight positional curves taken by the given geometric shape with the help of CAGD and used as boundary conditions. An illustrated solution of equation (8) with 8 boundary conditions is drawn in Figure 1 as representing the 3D model of an apple.

Let the domain of Ω be finite defined as Ω: $0 \leq \alpha \leq 1, 0 \leq \beta \leq 2\pi$ such that

$$\begin{aligned} \Omega(0, \beta) &= \hbar_0(\beta), \\ \Omega(k, \beta) &= \hbar_k(\beta), \\ \Omega(l, \beta) &= \hbar_l(\beta), \\ \Omega(m, \beta) &= \hbar_m(\beta), \\ \Omega(n, \beta) &= \hbar_n(\beta), \\ \Omega(o, \beta) &= \hbar_o(\beta), \\ \Omega(p, \beta) &= \hbar_p(\beta), \\ \Omega(1, \beta) &= \hbar_1(\beta), \end{aligned} \tag{9}$$

$\hbar_0(\beta), \hbar_k(\beta), \hbar_l(\beta), \hbar_m(\beta), \hbar_n(\beta), \hbar_0(\beta), \hbar_p(\beta), \hbar_1(\beta)$ are the boundary conditions. The relative position of the boundary curve depends on the parameters $0 < k < l < m < n < o < p < 1$.

Figure 1: 3D model of an apple.

In this research, equation (8) is solved by using the method of separation of variables as follows:

$$\Omega(\alpha,\beta) = \overline{\varrho}_0(\alpha) + \sum_{i=1}^{F}\left[\overline{\sigma}_i(\alpha)\cos(i\beta) + \overline{\tau}_i(\alpha)\sin(i\beta)\right], \tag{10}$$

where

$$\overline{\varrho}_0 = \overline{\mu}_{00} + \overline{\mu}_{01}\alpha + \overline{\mu}_{02}\alpha^2 + \overline{\mu}_{03}\alpha^3 + \overline{\mu}_{04}\alpha^4 + \overline{\mu}_{05}\alpha^5 + \overline{\mu}_{06}\alpha^6 + \overline{\mu}_{07}\alpha^7, \tag{11}$$

$$\overline{\sigma}_i = \overline{\nu}_{i1}e^{\eta i\alpha} + \overline{\nu}_{i2}e^{-\eta i\alpha} + \overline{\nu}_{i3}\alpha e^{\eta i\alpha} + \overline{\nu}_{i4}\alpha e^{-\eta i\alpha} + \overline{\nu}_{i5}\alpha^2 e^{\eta i\alpha} + \overline{\nu}_{i6}\alpha^2 e^{-\eta i\alpha} + \overline{\nu}_{i7}\alpha^3 e^{\eta i\alpha} + \overline{\nu}_{i8}\alpha^3 e^{-\eta i\alpha}, \tag{12}$$

$$\overline{\tau}_i = \xi_{i1}e^{\eta i\alpha} + \overline{\xi}_{i2}e^{-\eta i\alpha} + \xi_{i3}\alpha e^{\eta i\alpha} + \xi_{i4}\alpha e^{-\eta i\alpha} + \overline{\xi}_{i5}\alpha^2 e^{\eta i\alpha} + \overline{\xi}_{i6}\alpha^2 e^{-\eta i\alpha} + \xi_{i7}\alpha^3 e^{\eta i\alpha} + \xi_{i8}\alpha^3 e^{-\eta i\alpha}. \tag{13}$$

Here, all the values of $\mu, \nu,$ and ξ are unknown.

The effect in the final shape of a model due to these boundary conditions is shown in Figure 1. A slight change in the position of the curves can change the shape of the entire model. The unknown parameters, μ, ν, and ξ, also have a huge role in obtaining the final shape.

2.2. Error Analysis. The unknown constants are Fourier coefficients. They can be calculated using suitable numerical techniques on the given boundary conditions. The shape of the final model involves some error. The following equation shows that error:

$$\Omega(\alpha,\beta) = \overline{\varrho}_0(\alpha) + \sum_{i=1}^{F}\left[\overline{\sigma}_i(\alpha)\cos(i\beta) + \overline{\tau}_i(\alpha)\sin(i\beta)\right] + \overline{R}(\alpha,\beta), \tag{14}$$

where the error is shown by $\overline{R}$ and F is a finite natural number.

In the boundary conditions, the coefficients $\rho(\alpha)$ and $\tau(\alpha)$ can be calculated using the amplitude of the i^{th} mode. The role of high frequency modes to the final model is shown by the term $\overline{R}(\alpha,\beta)$. Because of the finite value of F, this term has an effect on the overall shape of the model. The following equation is used to find this term:

$$\overline{R}(\alpha,\beta) = \overline{\omega}_1(\beta)e^{l\alpha} + \overline{\omega}_2(\beta)e^{-l\alpha} + \overline{\omega}_3(\beta)\alpha e^{l\alpha} + \overline{\omega}_4(\beta)\alpha e^{-l\alpha} + \overline{\omega}_5(\beta)\alpha^2 e^{l\alpha} + \overline{\omega}_6(\beta)\alpha^2 e^{-l\alpha} + \overline{\omega}_7(\beta)\alpha^3 e^{l\alpha} + \overline{\omega}_8(\beta)\alpha^3 e^{-l\alpha}. \tag{15}$$

Here, $\overline{\omega}_1, \overline{\omega}_2, \overline{\omega}_3, \overline{\omega}_4, \overline{\omega}_5, \overline{\omega}_6, \overline{\omega}_7, \overline{\omega}_8$, and l are obtained, by taking the difference of the original boundary conditions with the conditions fulfilled by the function in equation (10).

2.3. Different Geometric Models Using PDE Surfaces. The various geometrical figures can be generated from a variety of curve options. The examples mentioned demonstrate the efficacy and comprehensibility of the PDE approach for the generation of complex geometry shapes, which supports the main goal of this study. The figures from 2 to 9 are generated using eight boundary conditions with Ω: $0 \leq \alpha \leq 1, 0 \leq \beta \leq 2\pi$, where $x = \alpha\cos(\beta), y = \alpha\sin(\beta)$ and $0 \leq z \leq 1$. In Figure 2, only a single point is taken for the first curve and the surface is generated by joining that point to each point of the next curve. Figure 3 is also generated using a point for top and bottom curves. A circular curve is used for the first curve of Figure 4 and a point for its bottom curve which gave it the shape of a pot. To generate the shape of a peach in Figure 5, the position of the first curve is taken between the second and third curves. (Figures 6–9) are also drawn in the same manner according to the related boundaries conditions.

3. Intelligent Systems for Designing of the Culinary Product Based on the Fuzzy Soft Partial Differential Equation

In optimum designing of the culinary product, the Bonferroni mean has the ability to capture desirable properties among arguments' interrelationship. While the fuzzy soft set deals with the situation where uncertainty occurs, differential equation is a useful tool to analyse the rate of change of dependent variables with respect to the independent variable. Therefore, the characteristic of BM with blend of fuzzy soft sets and differential equation becomes a very useful instrument to design an optimum culinary product according to the requirement of the industry. In this section, fuzzy soft matrix is used with weighted Bonferroni mean to calculate the value of the smoothness parameter, η, in the PDE defined in equation (8). An example is also developed to demonstrate the reliability of the developed technique.

3.1. An Intelligent System for Optimum Geometric Design. In the previous section, equation (8) was used to generate a PDE surface using eight curves. This equation has a parameter η, known as the smoothness parameter, which plays an important role in the shape and smoothness of a surface. Usually, η is considered 1 by default. But when this PDE method is applied to design a product for some customers, a specific value of η is needed as it plays an important role in fulfilling the requirements of the customer. The parameter, η, consists of all the specifications for designing a product, for example, price, quality, design, volume, and shape. Due to the uncertainty involved during product designing, it is not possible to take $\eta = 1$. To develop an intelligent system for designing the required product using η in the PDE given in equation (8) for different requirements of the industry, the following steps should be considered.

Step 1: there are r decision makers, who provide r number of decision matrices, in the form of fuzzy soft matrices $A^r_{mn} = [\mathrm{a_{mn}}]$, where $m = 1, 2, \ldots, i$ and $n = 1, 2, \ldots, j$, according to industrial requirements to design a specific product. A weight vector $W = \{w_1, w_2, w_3, \ldots, w_n\}$ is also given according to the industry requirements. W must satisfy the conditions $w_p > 0$ for $p = 1, 2, 3, \cdots, j$ and $\sum_{p=1}^{j} \omega_p = 1$, then using Definition 7, we calculate WBFSM for each $A_{mn} = [\mathrm{a_{mn}}]$. For each decision matrix Amn, a unique resultant matrix of the form WAs,t = $[\mathrm{a_{m1}}]$, for m = 1, 2, 3, . . ., i and s, t are natural numbers, are developed. Each entry of $WA^{s,t}$ (say η_{mn}) provides a unique product design by using Equation (8) as specified by the industry.

Step 2: a matrix $E = [\eta_{mn}]$, where $m = 1, 2, \cdots, i$ and $n = 1, 2, \cdots j$, will be generated by the calculated values of η_{mn} in step 1.

Step 3: to select the best product design between the generated designs by each η_{mn}, we use

$$\begin{aligned}&\text{Optimum Smoothing Parameter}\left(\eta^{-}\right)\\&\quad= \max\left(\max\left(\eta_{mn}\right)\right),\end{aligned} \tag{16}$$

where $m = 1, 2, \ldots, i$ and $n = 1, 2, \ldots, j$. This intelligent system helps obtain an optimal geometric design with the help of $\overline{\eta}$. This is the best design of the desired product which completely fulfills the requirements of the industry.

3.2. Illustrated Example. Mr. Khan is an owner of a juice bar, who wants to buy cold drink glass for serving fizzy drinks. He wants the design of the glass to be attractive but simple. Also, the glass should be of fine quality with price as low as possible, and the volume of the glass should be appropriate for one serving. He went to a glass design company. He selected five different basic designs for glass according to his given parameters which are $P = \{p(\text{price}), v(\text{volume}), \text{and } q(\text{quality})\}$. Mr. Khan also gave some weight $W = (0.4\ 0.3\ 0.3)$ to each of these parameters. Then, these designs were given to five experts de singers $= \{d_1, d_2, d_3, d_4, d_5\}$. All the designers gave their suggestions for each glass according to Mr. Khan's requirements. Following is the fuzzy soft matrix for the basic design of the first glass according to the suggestions of the experts.

$$G_1 = \begin{bmatrix} 0.30 & 0.70 & 0.20 \\ 0.90 & 0.60 & 0.70 \\ 0.60 & 0.75 & 0.40 \\ 0.80 & 0.60 & 0.50 \\ 0.40 & 0.50 & 0.35 \end{bmatrix}. \tag{17}$$

Then, using the definition (2.0.9) of weighted Bonferroni fuzzy soft matrix (WBFSM), the WBFSM for the first glass design G_1 is according to the given weights for the parameters, which is as follows:

$$B_1 = \begin{bmatrix} 0.1225 \\ 0.2437 \\ 0.1913 \\ 0.2102 \\ 0.1373 \end{bmatrix}. \tag{18}$$

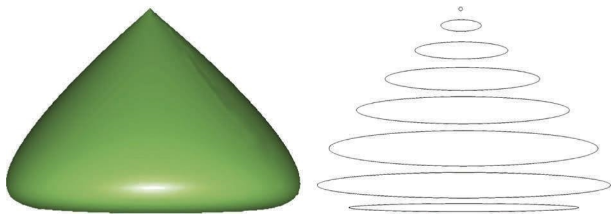

Figure 2: Tomb of a mosque with the following boundary condition in which $0 \le \beta \le 2\pi$: $C_1 = (0.0\cos(\beta), 0.0\sin(\beta), 1.0)$, $C_2 = (0.1\cos(\beta), 0.1\sin(\beta), 0.8)$, $C_3 = (0.3\cos(\beta), 0.3\sin(\beta), 0.7)$, $C_4 = (0.5\cos(\beta), 0.5\sin(\beta), 0.6)$, $C_5 = (0.6\cos(\beta), 0.6\sin(\beta), 0.5)$, $C_6 = (0.8\cos(\beta), 0.8\sin(\beta), 0.3)$, $C_7 = (0.9\cos(\beta), 0.9\sin(\beta), 0.2)$, and $C_8 = (0.7\cos(\beta), 0.7\sin(\beta), 0.0)$.

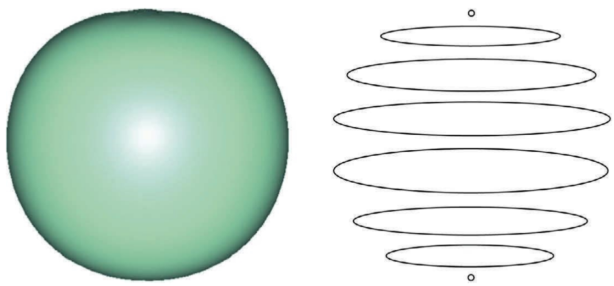

Figure 3: Sphere with the following boundary condition in which $0 \le \beta \le 2\pi$: $C_1 = (0.0\cos(\beta), 0.0\sin(\beta), 1.0)$, $C_2 = (0.2\cos(\beta), 0.2\sin(\beta), 0.8)$, $C_3(0.6\cos(\beta), 0.6\sin(\beta), 0.7)$, $C_4 = (1.0\cos(\beta), 1.0\sin(\beta), 0.5)$, $C_5 = (0.6\cos(\beta), 0.6\sin(\beta), 0.3)$, $C_6 = (0.2\cos(\beta), 0.2\sin(\beta), 0.2)$, $C_7 = (0.1\cos(\beta), 0.1\sin(\beta), 0.1)$, and $C_8 = (0.0\cos(\beta), 0.0\sin(\beta), 0.0)$.

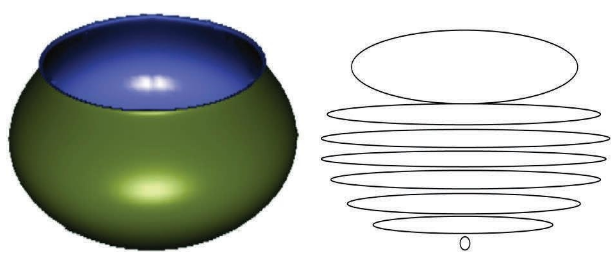

Figure 4: A cooking pot with the following boundary condition in which $0 \le \beta \le 2\pi$: $C_1 = (0.7\cos(\beta), 0.7\sin(\beta), 1.0)$, $C_2 = (0.5\cos(\beta), 0.5\sin(\beta), 0.95)$, $C_3 = (0.6\cos(\beta), 0.6\sin(\beta), 0.7)$, $C_4 = (0.7\cos(\beta), 0.7\sin(\beta), 0.6)$, $C_5 = (0.8\cos(\beta), 0.8\sin(\beta), 0.5)$, $C_6 = (1.0\cos(\beta), 1.0\sin(\beta), 0.4)$, $C_7 = (0.4\cos(\beta), 0.4\sin(\beta), 0.2)$, and $C_8 = (0.1\cos(\beta), 0.1\sin(\beta), 0.0)$.

Now, for matrix G_1, there are five different values. Each value defines a smoothness parameter η_{mn} for a separate glass. Each value will be used in equation (8) as η_{mn} to get a slightly different glass design. Here, the values are $\eta_{11} = 0.1225$, $\eta_{21} = 0.2437$, $\eta_{31} = 0.1913$, $\eta_{41} = 0.2102$, and $\eta_{51} = 0.1373$. Putting these values in equation (8), the following designs are generated:

As it can be seen from the data $\eta_{21} > \eta_{41} > \eta_{31} > \eta_{51} > \eta_{11}$, so the glass designed in Figure 10(b) with the value η_{21} is the best between these five glass designs described in Figures 10(a)–10(e). The difference between these glasses is

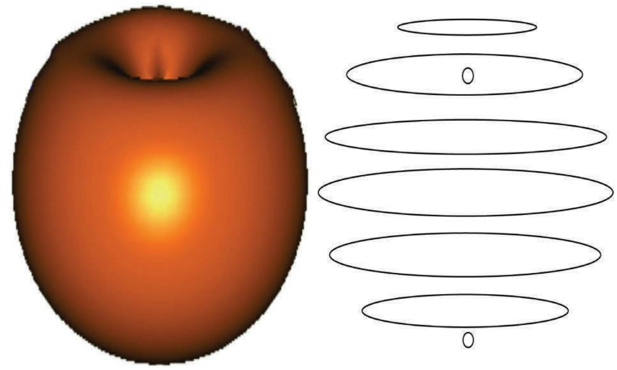

Figure 5: A peach model with the following boundary condition in which $0 \le \beta \le 2\pi$: $C_1 = (0.0\cos(\beta), 0.0\sin(\beta), 0.8)$, $C_2 = (0.3\cos(\beta), 0.3\sin(\beta), 1.0)$, $C_3 = (0.5\cos(\beta), 0.5\sin(\beta), 0.7)$, $C_4 = (0.8\cos(\beta), 0.8\sin(\beta), 0.6)$, $C_5 = (1.0\cos(\beta), 1.0\sin(\beta), 0.5)$, $C_6 = (0.8\cos(\beta), 0.8\sin(\beta), 0.3)$, $C_7 = (0.3\cos(\beta), 0.3\sin(\beta), 0.2)$, and $C_8 = (0.0\cos(\beta), 0.0\sin(\beta), 0.0)$.

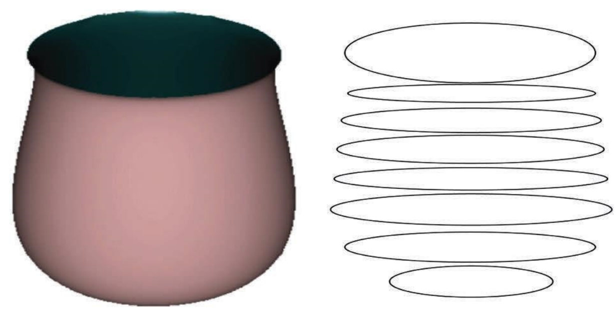

Figure 6: A glass bowl with the following boundary condition in which $0 \le \beta \le 2\pi$: $C_1 = (0.8\cos(\beta), 0.8\sin(\beta), 1.0)$ $C_2 = (0.7\cos(\beta), 0.7\sin(\beta), 0.9)$, $C_3 = (0.8\cos(\beta), 0.8\sin(\beta), 0.7)$, $C_4 = (0.85\cos(\beta), 0.85\sin(\beta), 0.6)$, $C_5 = (0.9\cos(\beta), 0.9\sin(\beta), 0.5)$, $C_6 = (1.0\cos(\beta), 1.0\sin(\beta), 0.3)$, $C_7 = (0.9\cos(\beta), 0.9\sin(\beta), 0.15)$, and $C_8 = (0.5\cos(\beta), 0.5\sin(\beta), 0.0)$.

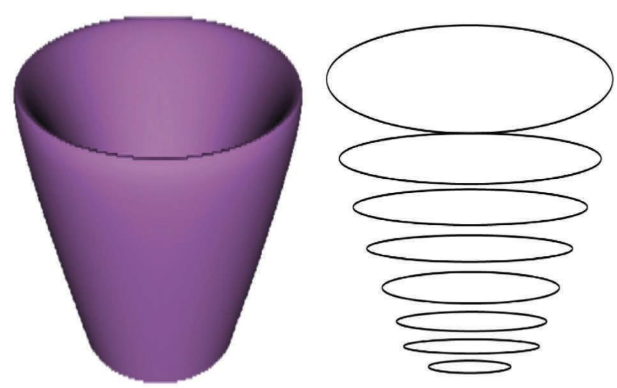

Figure 7: Drinking glass with the following boundary condition in which $0 \le \beta \le 2\pi$: $C_1 = (1.0\cos(\beta), 1.0\sin(\beta), 1.0)$, $C_2 = (0.9\cos(\beta), 0.9\sin(\beta), 0.8)$, $C_3 = (0.7\cos(\beta), 0.7\sin(\beta), 0.7)$, $C_4 = (0.6\cos(\beta), 0.6\sin(\beta), 0.6)$, $C_5 = (0.5\cos(\beta), 0.5\sin(\beta), 0.5)$, $C_6 = (0.4\cos(\beta), 0.4\sin(\beta), 0.3)$, $C_7 = (0.3\cos(\beta), 0.3\sin(\beta), 0.2)$, and $C_8 = (0.2\cos(\beta), 0.2\sin(\beta), 0.0)$.

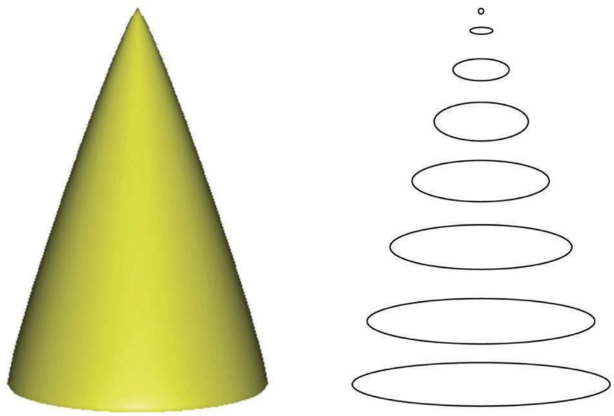

Figure 8: A cone model with the following boundary condition in which $0 \le \beta \le 2\pi$: $C_1 = (0.0\cos(\beta),\ 0.0\sin(\beta),\ 1.0)$, $C_2 = (0.1\cos(\beta),\ 0.1\sin(\beta),\ 0.9)$, $C_3 = (0.2\cos(\beta),\ 0.2\sin(\beta),\ 0.8)$, $C_4 = (0.4\cos(\beta),\ 0.4\sin(\beta),\ 0.6)$, $C_5 = (0.6\cos(\beta),\ 0.6\sin(\beta),\ 0.5)$, $C_6 = (0.8\cos(\beta),\ 0.8\sin(\beta),\ 0.3)$, $C_7 = (0.9\cos(\beta),\ 0.9\sin(\beta),\ 0.2)$, and $C_8 = (1.0\cos(\beta),\ 1.0\sin(\beta),\ 0.0)$.

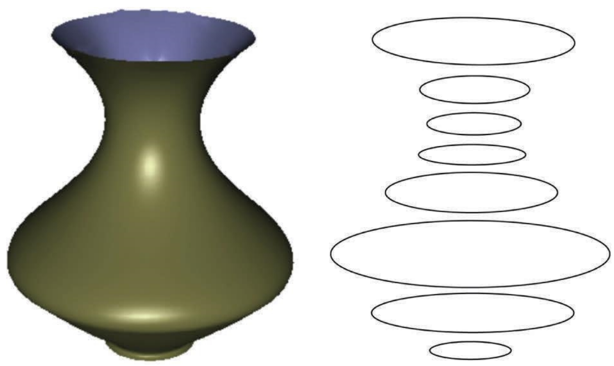

Figure 9: Vase with narrow mouth with the following boundary condition in which $0 \le \beta \le 2\pi$: $C_1 = (0.5\cos(\beta),\ 0.5\sin(\beta),\ 1.0)$, $C_2 = (0.3\cos(\beta),\ 0.3\sin(\beta),\ 0.8)$, $C_3 = (0.25\cos(\beta),\ 0.25\sin(\beta),\ 0.7)$, $C_4 = (0.3\cos(\beta),\ 0.3\sin(\beta),\ 0.6)$, $C_5 = (0.4\cos(\beta),\ 0.4\sin(\beta),\ 0.5)$, $C_6 = (0.75\cos(\beta),\ 0.75\sin(\beta),\ 0.3)$, $C_7 = (0.5\cos(\beta),\ 0.5\sin(\beta),\ 0.2)$, and $C_8 = (0.15\cos(\beta),\ 0.15\sin(\beta),\ 0.0)$.

so small that one cannot detect it just by looking at their pictures, but when the data are observed, it can be seen that the glass with the best quality and moderate volume is selected. Here, volume of 0.5 is approximately equal to 250 ml that is also considered as one serving of a drink. If the given data of Figure 10(e) are observed, it has the exact volume of one serving, but the quality of the material of glass is very low, so it is not a good choice for the customer.

The fuzzy soft matrix for the second design of the glass according to the suggestions of the experts is as follows:

$$G_2 = \begin{bmatrix} 0.10 & 0.65 & 0.30 \\ 0.60 & 0.53 & 0.70 \\ 0.40 & 0.60 & 0.50 \\ 0.50 & 0.57 & 0.60 \\ 0.80 & 0.48 & 1.00 \end{bmatrix}. \tag{19}$$

Similarly, WBFSM for the matrix G_2 is as follows:

$$B_2 = \begin{bmatrix} 0.0982 \\ 0.2016 \\ 0.1631 \\ 0.1835 \\ 0.2485 \end{bmatrix}. \tag{20}$$

Here, $\eta_{12} = 0.0982$, $\eta_{22} = 0.2016$, $\eta_{32} = 0.1631$, $\eta_{42} = 0.1835$, and $\eta_{52} = 0.2485$. Putting these values of η_{mn} in equation (8), the generated designs are as follows:

Here, $\eta_{52} > \eta_{22} > \eta_{42} > \eta_{32} > \eta_{12}$. So, η_{52} gives the best glass from the abovementioned five glasses shown in Figures 11(a)–11(e). It can be noticed from the data that η_{52} has the highest quality and moderate volume for one serving.

The fuzzy soft matrix for the third glass design is as follows:

$$G_3 = \begin{bmatrix} 0.20 & 0.25 & 0.35 \\ 0.70 & 0.58 & 0.50 \\ 1.00 & 0.48 & 0.65 \\ 0.40 & 0.25 & 0.50 \\ 0.10 & 0.10 & 0.30 \end{bmatrix}. \tag{21}$$

For matrix G_3, the WBFSM is as follows:

$$B_3 = \begin{bmatrix} 0.0862 \\ 0.1973 \\ 0.2336 \\ 0.1255 \\ 0.0500 \end{bmatrix}. \tag{22}$$

Here, $\eta_{13} = 0.0862$, $\eta_{23} = 0.1973$, $\eta_{33} = 0.2336$, $\eta_{43} = 0.1255$, and $\eta_{53} = 0.0500$. Figures 12(a)–12(e) designs are generated by the values of η_{mn} after putting them in equation (8):

As $\eta_{33} > \eta_{23} > \eta_{43} > \eta_{13} > \eta_{53}$, so the selected design for G_3 seen in Figure 12(c) is the design made by η_{33}. This design has the highest quality, and the volume is close to 250 ml.

Now, for the fourth glass design, the fuzzy soft matrix is as follows:

$$G_4 = \begin{bmatrix} 0.20 & 0.10 & 0.30 \\ 0.80 & 0.60 & 0.50 \\ 0.40 & 0.37 & 0.60 \\ 0.10 & 0.20 & 0.10 \\ 1.00 & 0.40 & 0.80 \end{bmatrix}. \tag{23}$$

The weighted Bonferroni fuzzy soft matrix (WBFSM) for fuzzy soft matrix G_4 is as follows:

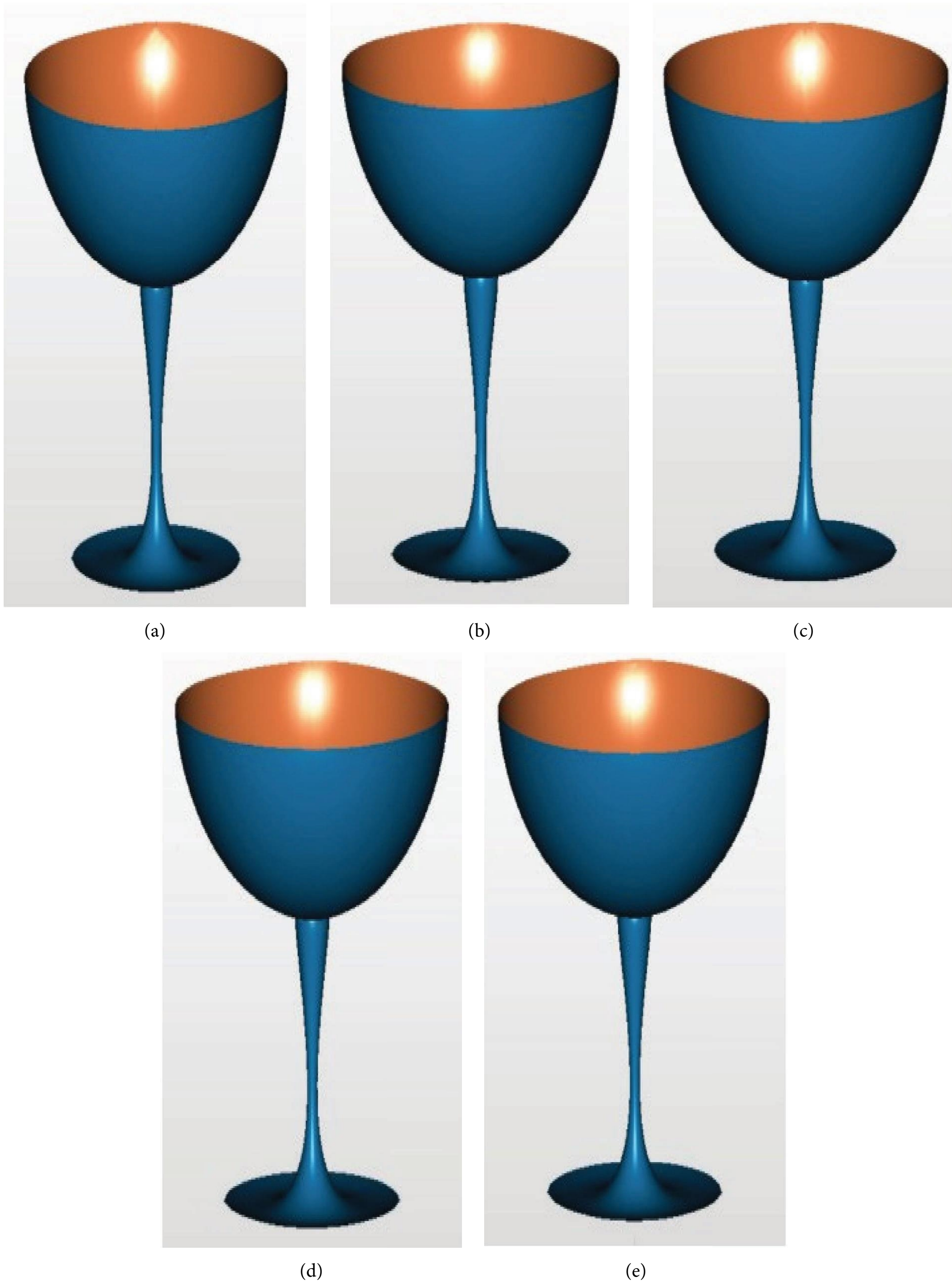

FIGURE 10: (a) First glass model when the smoothness parameter is $\eta_{11} = 0.1225$. (b) First glass model when the smoothness parameter is $\eta_{21} = 0.2437$. (c) First glass model when the smoothness parameter is $\eta_{31} = 0.1913$. (d) First glass model when the smoothness parameter is $\eta_{41} = 0.2102$. (e) First glass model when the smoothness parameter is $\eta_{51} = 0.1373$.

$$B_4 = \begin{bmatrix} 0.0640 \\ 0.2102 \\ 0.1489 \\ 0.0424 \\ 0.2400 \end{bmatrix}. \tag{24}$$

$\eta_{14} = 0.0640$, $\eta_{24} = 0.2102$, $\eta_{34} = 0.1489$, $\eta_{44} = 0.0424$, and $\eta_{54} = 0.2400$. Putting these values in equation (8) for η_{mn}gives slightly different designs.

$\eta_{54} > \eta_{24} > \eta_{34} > \eta_{14} > \eta_{44}$. Similarly, by observing the data given for this design, it is noticed that η_{54} has the finest quality with volume closer to 250 ml. So, the glass generated

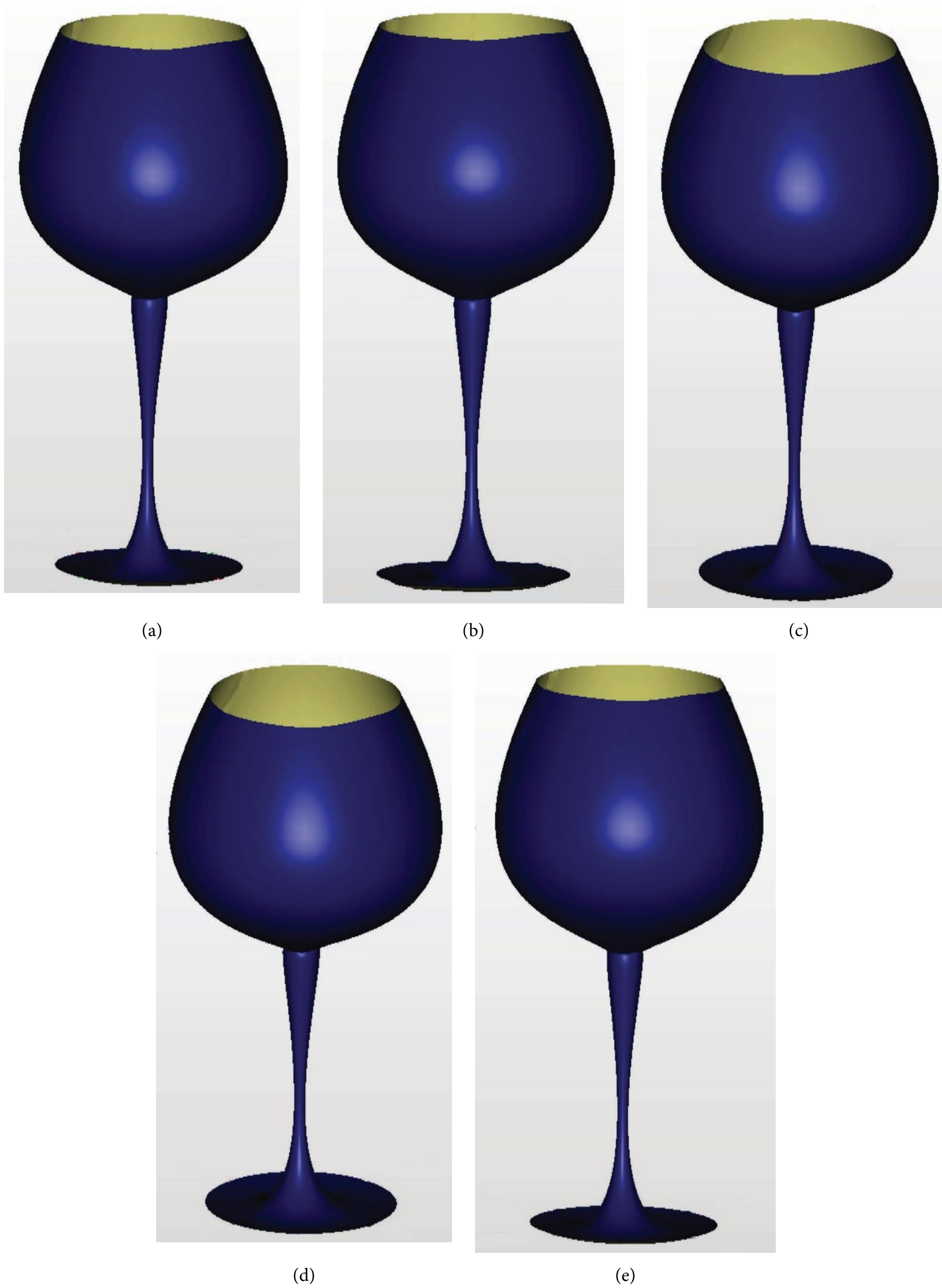

FIGURE 11: (a) Second glass model when the smoothness parameter is $\eta_{12} = 0.0982$. (b) Second glass model when the smoothness parameter is $\eta_{22} = 0.2016$. (c) Second glass model when the smoothness parameter is $\eta_{32} = 0.1631$. (d) Second glass model when the smoothness parameter is $\eta_{42} = 0.1835$. (e) Second glass model when the smoothness parameter is $\eta_{52} = 0.2485$.

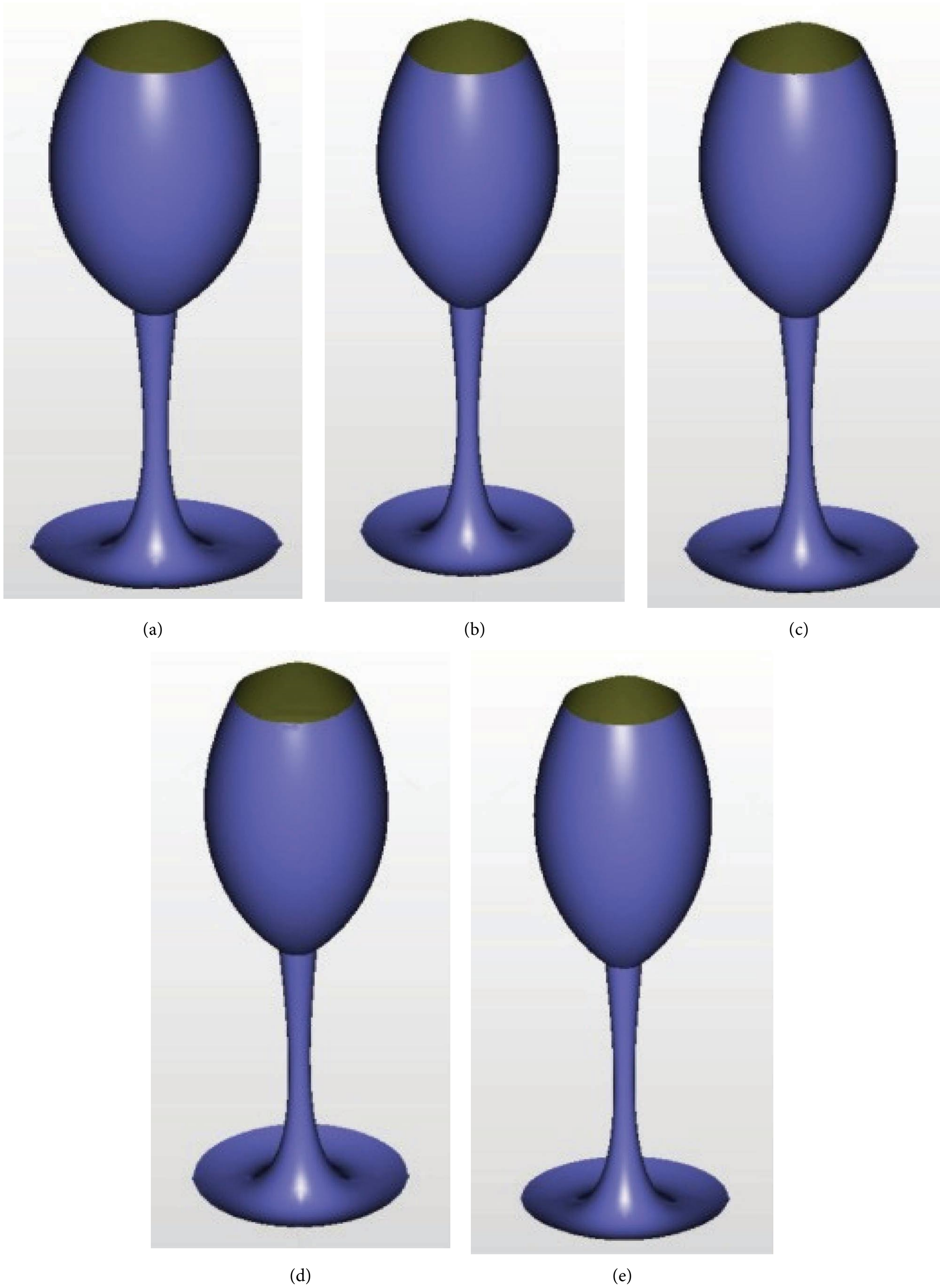

Figure 12: (a) Third glass model when the smoothness parameter is $\eta_{13} = 0.0862$. (b) Third glass model when the smoothness parameter is $\eta_{23} = 0.1973$. (c) Third glass model when the smoothness parameter is $\eta_{33} = 0.2336$. (d) Third glass model when the smoothness parameter is $\eta_{43} = 0.1255$. (e) Third glass model when the smoothness parameter is $\eta_{53} = 0.0500$.

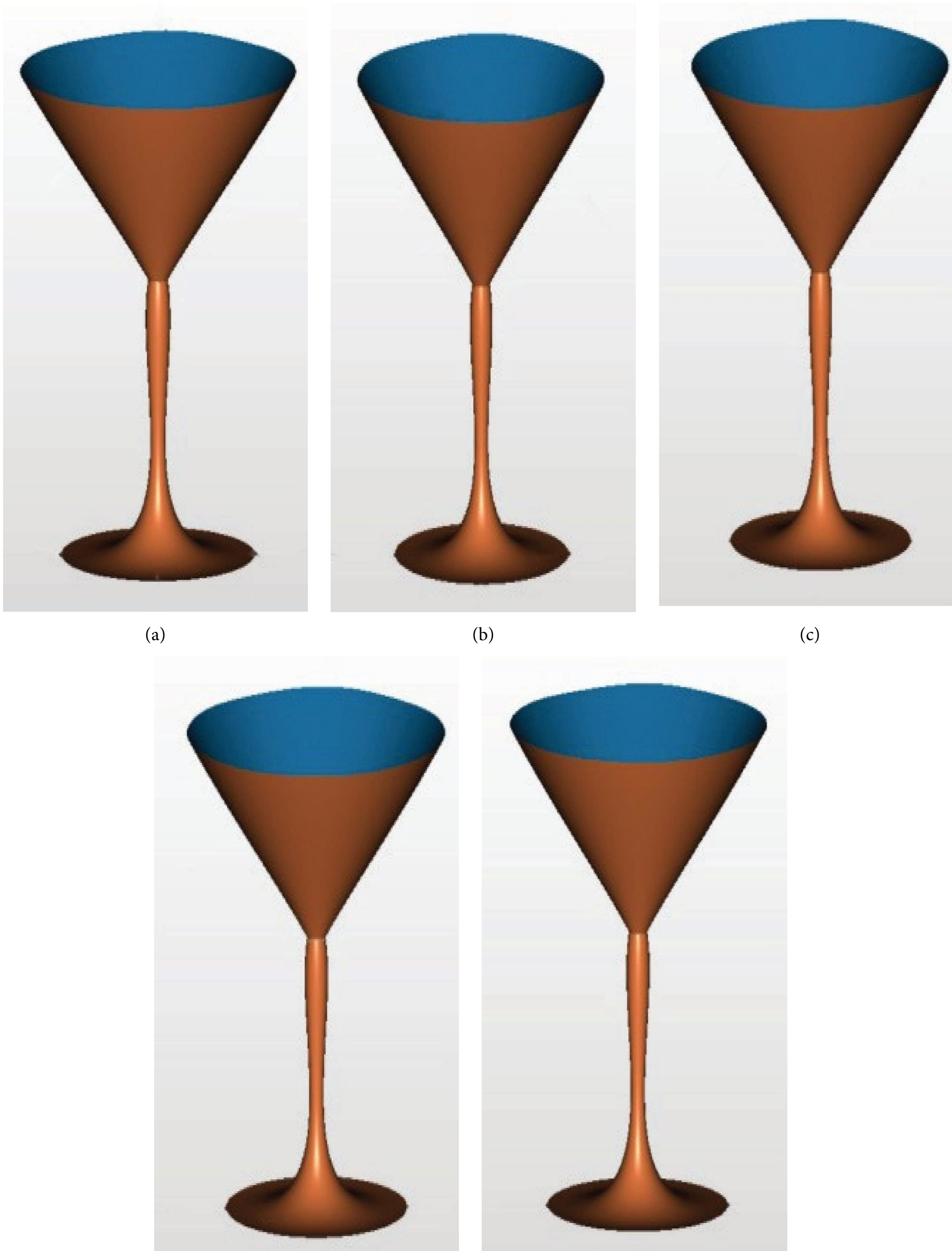

(a) (b) (c)

(d) (e)

FIGURE 13: (a) Forth glass model when the smoothness parameter is $\eta_{14} = 0.0640$. (b) Forth glass model when the smoothness parameter is $\eta_{24} = 0.2102$. (c) Forth glass model when the smoothness parameter is $\eta_{34} = 0.1489$. (d) Forth glass model when the smoothness parameter is $\eta_{44} = 0.0424$. (e) Forth glass model when the smoothness parameter is $\eta_{54} = 0.2400$.

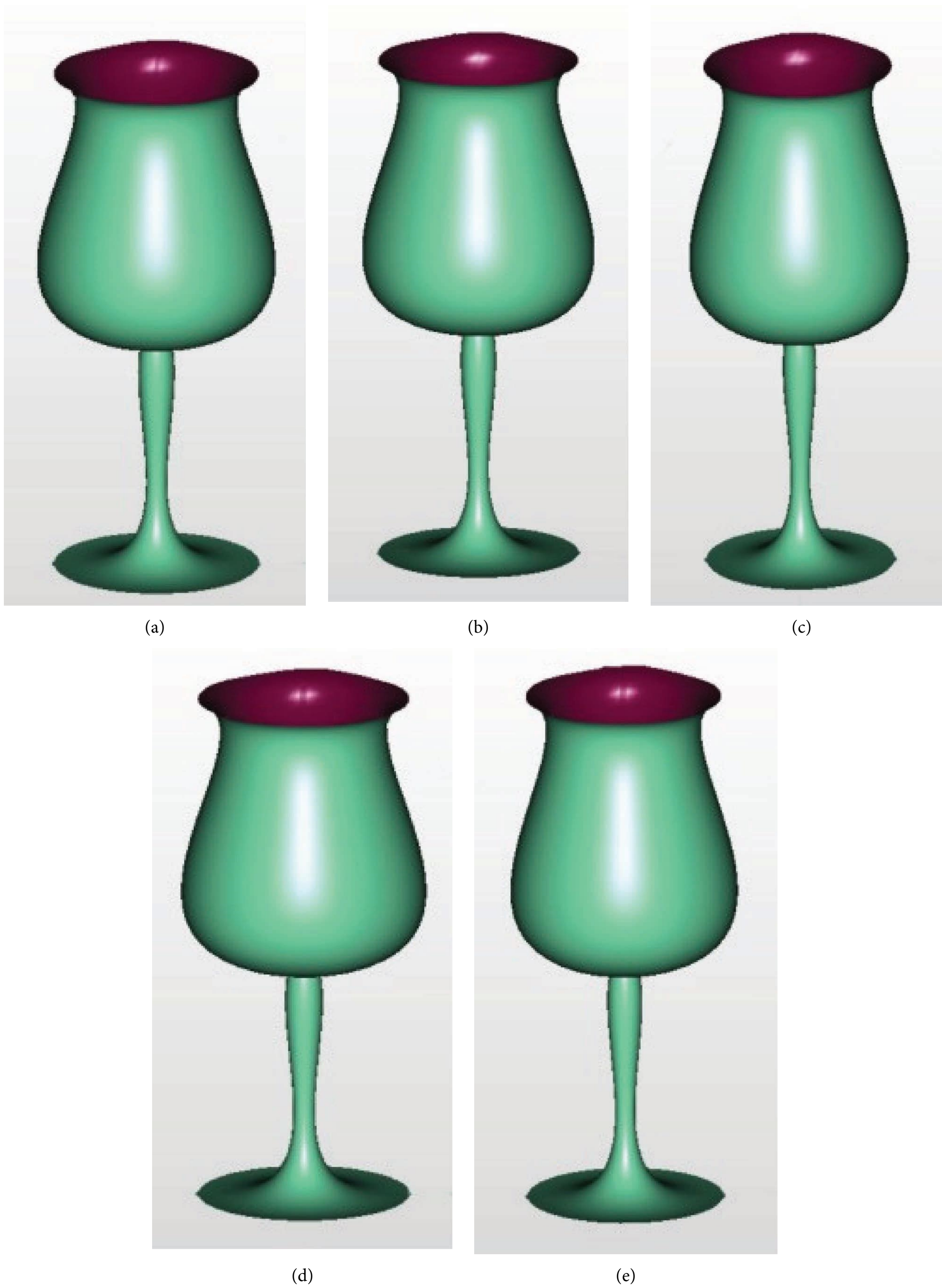

Figure 14: (a) Fifth glass model when the smoothness parameter is $\eta_{15} = 0.2163$. (b) Fifth glass model when the smoothness parameter is $\eta_{25} = 0.2365$. (c) Fifth glass model when the smoothness parameter is $\eta_{35} = 0.1741$. (d) Fifth glass model when the smoothness parameter is $\eta_{45} = 0.1494$. (e) Fifth glass model when the smoothness parameter is $\eta_{55} = 0.1192$.

in Figure 13(d), with η_{54}, is the selected glass from the glass design for G_4 shown in Figures 13(a)–13(e).

Fuzzy soft matrix for the last glass design according to the suggestions of the designers is as follows:

$$G_5 = \begin{bmatrix} 0.90 & 0.30 & 0.80 \\ 1.00 & 0.35 & 0.83 \\ 0.60 & 0.70 & 0.30 \\ 0.50 & 0.63 & 0.25 \\ 0.40 & 0.20 & 0.50 \end{bmatrix}. \quad (25)$$

Now, for this last fuzzy soft matrix G_5, WBFSM is as follows:

$$B_5 = \begin{bmatrix} 0.2163 \\ 0.2365 \\ 0.1741 \\ 0.1494 \\ 0.1192 \end{bmatrix}. \quad (26)$$

Here, $\eta_{15} = 0.2163$, $\eta_{25} = 0.2365$, $\eta_{35} = 0.1741$, $\eta_{45} = 0.1494$, and $\eta_{55} = 0.1192$. Putting these values for η_{mn} in equation (8) gives slightly different designs shown in Figures 14(a)–14(e):

$\eta_{25} > \eta_{15} > \eta_{35} > \eta_{45} > \eta_{55}$. Here, η_{25} has the greatest value, so it is our selected glass for G_5. The selected glass shown in Figure 14(b) has volume closer to 250 ml and finest quality.

Now, all the values of η_{mn} will generate a matrix such that

$$\begin{bmatrix} 0.1225 & 0.0982 & 0.0862 & 0.0640 & 0.2163 \\ 0.2437 & 0.2016 & 0.1973 & 0.2102 & 0.2365 \\ 0.1913 & 0.1631 & 0.2336 & 0.1489 & 0.1741 \\ 0.2102 & 0.1835 & 0.1255 & 0.0424 & 0.1494 \\ 0.1373 & 0.2485 & 0.0500 & 0.2400 & 0.1192 \end{bmatrix}. \quad (27)$$

A maximum value has been selected from each column of the abovementioned matrix, and by the definition of the optimum smoothness parameter, $\overline{\eta}_{mn}$ defined in Step 3 will be used, which is as follows:

$$\begin{aligned} \overline{\eta} &= \max(0.2437, 0.2485, 0.2336, 0.2400, 0.2365), \\ \overline{\eta} &= 0.2485. \end{aligned} \quad (28)$$

As $\overline{\eta} = 0.2485$, so the glass design generated from this value is the best design according to the customer's requirement. If the data of the glass designs mentioned previously are observed, it can be seen that the final selected design has the lowest price and finest quality among all the five designs. Also, the volume of the selected glass design is slightly less than 250 ml, which is in the favor of our customer. The shape of the designed glass is also favorable for fizzy drinks. According to the case study about glass design on drinking behavior discussed in [38], it can be concluded that the selected design has the best effect on the drinking behavior of a person since the selected glass design has the curve that makes it easy for a person to take a sip of his drink. Also, its shape does not allow the fizz in the drink to die down immediately, so a person can enjoy his drink for a long time. Hence, the selected glass design has the best result in the favor of the customer, and it also fully satisfies his requirements.

From the influence of each glass design on the drinking behavior of a person, it can be proved that the selected glass is the best choice for Mr. Khan. Looking at the design of G_1 glass, it can be seen that it is shaped like a parabola. It also has a wide mouth, which makes it easier for a person to drink from it. Although it is a good shape of glass to serve juices, but it is not an ideal shape for fizzy drinks since it does not hold the fizz in the drink for a long time. Due to its wide mouth and parabolic shape, the fizz in the drink dies down fast. The design of glass G_3 is like a cylinder. Although it has a curve in its shape, which makes it a good choice for fizzy drinks, but its mouth is so narrow which makes it difficult for a person to drink from it. Its narrow mouth and low volume does not make it a good choice for fizzy drinks, but it is a good choice for alcoholic drinks because these types of glasses reduce the consumption of alcoholic drinks which is also mentioned in a case study on drinking behaviors [38]. The next glass design G_4 is a V-shaped glass. As it can be seen in the figure mentioned previously, this glass has a wide mouth with no curve in its shape, which makes it a bad choice for fizzy drinks. The reason for this glass not being a good choice for fizzy drinks is the same as the design of glass G_1, but unlike glass design G_1, it has a small volume, which makes it a good choice for nonfizzy drinks taken in small quantity. They are also a good choice for small serving of juice for kids. The glass design G_5 has a design like a vase or a tulip flower. Although it has an attractive shape, its deep curve and narrow mouth does not make it a good choice for fizzy drinks. This type of glasses is best for serving milk drinks such as milk shakes or coconut milk. Now, on observing the selected design of the glass which is G_2 glass design, it is clear that its shape is the ideal shape for fizzy drinks. It has a right amount of curve to hold the fizz in the drink for a long time and its mouth is not narrow, which allow a person to drink from it easily and enjoy his drink. On observing all the designs of the glasses, it is proven that the selected glass not only has the best shape for fizzy drinks but also fulfills the requirements of the customer, Mr. Khan.

4. Conclusion

In this article, an intelligent system is developed for geometric designing of products according to industrial requirements. This intelligent system is developed using the fuzzy soft partial differential equation with weighted Bonferroni mean to design the geometric models of the required product. For this purpose, a parameter known as the optimum smoothness parameter is defined, using WBFSM, in the PDE. This parameter fulfills industrial requirements and generates the optimal design of the desired product. The overall shape of the surface is determined by the boundary conditions (which are effectively defined by curves in 3-space) at the edge of the surface patch. As a result, it is relatively simple for a designer to use this intelligent system to create objects of practical significance using standard computer devices. As this intelligent system uses close curves, rather than using standard shapes, such as ellipse, square, and cylinder, it is easier to shape it according to the need. Finally, to show the effectiveness of the developed technique, an illustrated example is developed for the hotel industry to design a drinking glass according to their requirements. From these geometric designs of the glasses, the design developed using the optimum smoothness parameter was selected, as it fulfilled the customer's requirements in the best way possible. All of this process was performed prior to the development of the product, which reduced the time and money spent on the development of the glass.

The developed intelligent system of PDE with weighted Bonferroni fuzzy soft matrix can be useful in many industries. In the future, this developed system can further be extended in the development of many products. It can be used in the development of capsule shells in pharmaceutical companies because temperature has a major effect on these capsule shells. Extreme temperature can melt them, so this PDE method can be used by taking temperature as the main parameter. Similarly, it can also be used in the manufacturing of robots, aircrafts, and home decor products.

Data Availability

The datasets generated during and/or analyzed during the current study are available from the corresponding author upon reasonable request.

Additional Points

Human and Animal Rights. We would like to mention that this article does not contain any studies with animals and does not involve any studies on human beings.

Conflicts of Interest

The authors declare that they have no conflicts of interest.

Authors' Contributions

The authors equally conceived the study, participated in its design and coordination, drafted the manuscript, participated in the sequence alignment, and read and approved the final manuscript.

References

[1] M. M. M. Sarcar, K. M. Rao, and K. L. Narayan, *Computer Aided Design and Manufacturing*, PHI Learning Pvt. Ltd, New Delhi, 2008.

[2] J. Bear, "Conceptual and mathematical modeling," in *Seawater Intrusion in Coastal Aquifers—Concepts, Meth- Ods and Practices*, pp. 127–161, Springer, Berlin, Germany, 1999.

[3] M. O'Rourke, *Principles of Three-Dimensional Computer Animation: Modeling, Rendering, and Animating with 3D Computer Graphics*, WW Norton & Company, NewYork, NY, USA, 2003.

[4] A. Elnagar and A. Basu, "From 2d surface patches to 3d reconstructed models: theory and applications," *Pattern Recognition*, vol. 31, no. 10, pp. 1419–1430, 1998.

[5] P. J. Frey and H. Borouchaki, "Geometric surface mesh optimization," *Computing and Visualization in Science*, vol. 1, no. 3, pp. 113–121, 1998.

[6] G. Farin, *Curves and Surfaces for Computer-Aided Geometric Design: A Practical Guide*, Elsevier, Amsterdam, Netherlands, 2014.

[7] C. H. Chu and C. H. Séquin, "Developable bézier patches: properties and design," *Computer-Aided Design*, vol. 34, no. 7, pp. 511–527, 2002.

[8] B. F. Gregorski, B. Hamann, and K. I. Joy, "Reconstruction of b-spline surfaces from scattered data points," in *Proceedings of the computer graphics international 2000*, pp. 163–170, IEEE, Geneva, Switzerland, June 2000.

[9] A. Hertzmann and D. Zorin, "Illustrating smooth surfaces," in *Proceedings of the 27th annual conference on Computer graphics and interactive techniques*, pp. 517–526, New Orleans, LA, USA, July 2000.

[10] B. Sharp, "Subdivision surface theory," *Game Developer*, vol. 7, no. 1, pp. 34–42, 2000.

[11] J. Stam, "Loop C. Quad/triangle subdivision," in *Computer Graphics Forum*, pp. 79–85, Wiley Online Library, Hoboken, NJ, 2003.

[12] I. Malcolm Bloor and M. J. Wilson, "Spectral approximations to pde surfaces," *Computer-Aided Design*, vol. 28, no. 2, pp. 145–152, 1996.

[13] H. Ugail, "Time-Dependent Shape Parameterisation of Complex Geometry using PDE Surfaces," in *Geometric Modelling and Computing*, M. L. Lucian and M. Neamtu, Eds., pp. 501–512, Nashboro Press, 2004.

[14] H. Ugail and M. J. Wilson, "Efficient shape parametrisation for automatic design optimisation using a partial differential equation formulation," *Computers & Structures*, vol. 81, no. 28-29, pp. 2601–2609, 2003.

[15] L. Schumaker, *Spline Functions: Basic Theory*, John willey and sons. Inc, New York, NY, USA, 1981.

[16] C. D. Woodward, "Skinning techniques for interactive b-spline surface interpolation," *Computer-Aided Design*, vol. 20, no. 8, pp. 441–451, 1988.

[17] P. Bezier, *The Mathematical Basis of the UNIURF CAD System*, Butterworth-Heinemann, Oxford, UK, 2014.

[18] W. Tiller, "Rational b-splines for curve and surface representation," *IEEE Computer Graphics and Applications*, vol. 3, no. 6, pp. 61–69, 1983.

[19] H. Ugail, M. I. Bloor, and M. J. Wilson, "Manipulation of PDE surfaces using an interactively defined parameterisation," *Computers & Graphics*, vol. 23, no. 4, pp. 525–534, 1999.

[20] H. Ugail, M. I. Bloor, and M. J. Wilson, "Techniques for interactive design using the PDE method," *ACM Transactions on Graphics*, vol. 18, no. 2, pp. 195–212, 1999.

[21] M. I. Bloor and M. J. Wilson, "Using partial differential equations to generate free form surfaces," *Computer-Aided Design*, vol. 22, no. 4, pp. 202–212, 1990.

[22] H. Ugail and S. Kirmani, "Shape reconstruction using partial differential equations," *WSEAS Transactions on Computers*, vol. 10, no. 5, pp. 2156–2161, 2006.

[23] M. I. G. Bloor and M. J. Wilson, "Interactive design using partial differential equations," in *Designing Fair Curves and Surfaces: Shape Quality in Geometric Modeling and Computer-Aided Design*, pp. 231–251, SIAM, Kerala, 1994.

[24] H. Ugail, N. Jamil, and R. Satinoianu, "Method of numerical simulation of stable structures of fluid membranes and vesicles," *WSEAS Transactions on Mathematics*, vol. 5, no. 9, 2006.
[25] L. A. Zadeh, "Fuzzy sets," in *Fuzzy Sets, Fuzzy Logic, and Fuzzy Systems: Selected Papers by Lotfi A Zadeh*, pp. 394–432, World Scientific, Singapore, 1996.
[26] D. Molodtsov, "Soft set theory—first results," *Computers & Mathematics with Applications*, vol. 37, no. 4-5, pp. 19–31, 1999.
[27] P. K. Maji, R. Biswas, and A. R. Roy, "Soft set theory," *Computers & Mathematics with Applications*, vol. 45, no. 4-5, pp. 555–562, 2003.
[28] P. K. Maji, A. R. Roy, and R. Biswas, "Fuzzy soft sets," *Journal of Fuzzy Mathematics*, vol. 9, pp. 589–602, 2001.
[29] T. J. Neog and D. K. Sut, "Application of fuzzy soft sets in decision making problems using fuzzysoft matrices," *International Journal of Math Arch*, vol. 2.
[30] D. K. Sut, "An application of fuzzy soft relation in decision making problems," *International Journal of Mathematics Trends and Technology*, vol. 3, no. 2, pp. 51–54, 2012.
[31] N. Cagman, S. Enginoglu, and F. Citak, "Fuzzy parameterized fuzzy soft set theory and its applications," *Turkish Journal of Fuzzy System*, vol. 1, no. 1, pp. 21–35, 2010.
[32] Y. Celik and S. Yamak, "Fuzzy soft set theory applied to medical diagnosis using fuzzy arithmetic operations," *Journal of Inequalities and Applications*, vol. 2013, no. 1, pp. 82–89, 2013.
[33] I. Beg, T. Rashid, and R. N. Jamil, "Human attitude analysis based on fuzzy soft differential equations with bonferroni mean," *Computational and Applied Mathematics*, vol. 37, no. 3, pp. 2632–2647, 2018.
[34] C. Bonferroni, "Sulle medie multiple di potenze," *Bollettino dell'Unione Matematica Italiana*, vol. 5, no. 3-4, pp. 267–270, 1950.
[35] R. R. Yager, "On generalized bonferroni mean operators for multi-criteria aggregation," *International Journal of Approximate Reasoning*, vol. 50, no. 8, pp. 1279–1286, 2009.
[36] R. R. Yager, "On ordered weighted averaging aggregation operators in multicriteria decisionmaking," *IEEE Transactions on systems, Man, and Cybernetics*, vol. 18, no. 1, pp. 183–190, 1988.
[37] G. Beliakov, S. James, J. Mordelova, T. Rückschlossová, and R. R. Yager, "Generalized bonferroni mean operators in multi-criteria aggregation," *Fuzzy Sets and Systems*, vol. 161, no. 17, pp. 2227–2242, 2010.
[38] T. Langfield, R. Pechey, P. T. Gilchrist, M. Pilling, and T. M. Marteau, "Glass shape influences drinking be- haviours in three laboratory experiments," *Scientific Reports*, vol. 10, no. 1, pp. 13362–13411, Article ID 13362, 2020.
[39] A. R. Roy and P. K. Maji, "A fuzzy soft set theoretic approach to decision making problems," *Journal of compu- tational and Applied Mathematics*, vol. 203, no. 2, pp. 412–418, 2007.
[40] H. Dyckhoff and W. Pedrycz, "Generalized means as model of compensative connectives," *Fuzzy Sets and Systems*, vol. 14, no. 2, pp. 143–154, 1984.
[41] J. R. Woodwark and M. R. R. Blends, "The mathematics of surfaces," *Geometric Modelling*, Oxford Uni- versity Press, Oxford, UK.
[42] M. I. G. Bloor and M. J. Wilson, "Generating blend surfaces using partial differential equations," *Computer-Aided Design*, vol. 21, no. 3, pp. 165–171, 1989.